Prediction of a Heavy Rainfall Event over Taiwan Using Limited-Area Models

Ying-Hwa Kuo
National Center for Atmospheric Research
P.O. Box 3000, Boulder, CO 80307, U.S.A.

Project Period: 1 July 1991 to 30 June 1992

A research report submitted to the
Central Weather Bureau
Ministry of Communications
Republic of China

May 25, 1992

Executive Summary

In this study we continue to examine factors that are important to heavy rainfall prediction over the Taiwan area using limited-area models. Both the Central Weather Bureau's Limited-Area Forecast Systems (RFS and MFS) and the NCAR/Penn State mesoscale model MM4 were used to simulate a heavy rainfall event that occurred in TAMEX IOP#13. This project was carried out in collaboration with Dr. Yueh-Jiuan Hsu at the CWB. During the past year (from 1 July 1991 through 30 June 1992) several research activities were accomplished:

a. We performed a total of nine numerical experiments using the MM4 model. The results of these experiments were presented in this report.
b. Some results of this project were presented in an international conference (Ninth Conference on Numerical Weather Prediction). A reprint is enclosed (Hsu et al. 1991).
c. We invited Dr. Hsu to visit NCAR for a month (October 1991). During this month we worked with Dr. Hsu on the preparation of conference presentation, the precipitation verification for TAMEX IOP#13, and the model diagnosis using the interactive graphic analysis package--SIGMA. A version of SIGMA package was brought back by Dr. Hsu from NCAR to CWB.
d. We worked with Dr. Hsu on further numerical experiments using the CWB models. The results of these experiments were summarized in a paper presented at the 1992 Conference on Weather Analysis and Forecasting (reprint attached).

The key conclusions obtained from the nine numerical experiments performed at NCAR can be summarized as following:

1. Increase the vertical resolution from 15 levels to 23 levels had little impact on the results of 90-km, 45-km and 22.5-km models. The main reason for the lack of impact was due to the fact that most of the increase in vertical resolution took place in the middle and upper troposphere. For the simulation of the TAMEX IOP#13, it was the low-level frontal forcing and its interaction with the topography that was crucial for heavy precipitation. We note that the impact, though not large, increased with increased horizontal resolution. For numerical weather prediction over Taiwan, an improvement in horizontal resolution from 45-km to a grid size of at least 22.5 km is crucial. The improvement in vertical resolution is not as important. We recommend adding a few levels in the lower troposphere for the CWB models.
2. Test of different precipitation parameterizations on a 22.5 km model revealed considerable forecast sensitivity. Not only the precipitation amount and precipitation distribution were affected, the mesoscale pressure and wind fields were also affected. Among the three precipitation parameterizations tested, the Kuo scheme coupled with a simple nonconvective precipitation parameterization produced the best pressure and wind field distribution, while the Arakawa-Schubert scheme produced better precipitation distribution and amount. The Grell scheme combined with the more sophisticated explicit moisture scheme gave the worst results. Although the Kuo-

scheme appears to be quite adequate for this case, it is possible that further tuning of the Arakawa-Schubert scheme and the Grell scheme can improve their performance. Considerably more testing is required before a definite conclusion can be given.

3. The removal of the Taiwan's orography produced significant changes on the model simulation. A comparison of experiments with and without the orography of Taiwan indicates that the effect of the Central Mountain Range was to: (1) split the Mei-Yu front into eastern and western sections, (2) block the low-level southwesterly monsoon flow, (3) cause the middle-level low θ_e air to descend to the lee of the Central Mountain Range, (4) enhance the temperature and θ_e gradient of the Mei-Yu front to the west of Taiwan, and (5) produce enhanced precipitation on the upwind side of the mountain by blocking and lifting the warm, moist monsoon air. The importance of the CMR on the flow field, pressure field and precipitation distribution again calls for the use of high resolution models for numerical weather prediction in Taiwan. Only with high horizontal resolution can the CMR be properly represented in the model.
4. The use of nonhydrostatic mesoscale model at a horizontal resolution of 22.5 km produced moderate improvement in the model simulation. The cold air damming along the China coast and the meso-lows located off the northwestern coast and southeastern coast of Taiwan were all simulated with improved accuracy. Also, the precipitation amount produced by the

nonhydrostatic model was closer to the observed amount. More significantly, our results indicate that it is feasible to use nonhydrostatic mesoscale model for numerical weather prediction in Taiwan.

5. Detailed model diagnoses were performed on the results of E22.5L15 experiment. Vertical cross sections perpendicular to the front indicates extreme shallowness of the cold air behind the Mei-Yu front. The frontal slope was about 0.3/100. The shallowness of the cold air might explain the difficulties encountered by CWB's RFS and MFS in the simulation of the Mei-Yu front and its movement, in particular if the lowest three-levels were assumed to be well-mixed. The model diagnosis also indicates thermally direct secondary circulation across the Mei-Yu front. The heavy precipitation was found to take place within the warm, moist southwesterly monsoon flow, approximately 100 km ahead of the front. The model results suggest that as the Mei-Yu front advanced southward, the warm, moist monsoon air was forced to rise over west central Taiwan (near Taichung), as it was blocked by the Central Mountain Range to the east and the cold air to the north. The pre-frontal nature of the simulated heavy precipitation was consistent with the Doppler radar observation of the TAMEX IOP#13 pre-frontal squall line.

1. Introduction

This report summarizes the work performed during the period of July 1 1991 to June 30 1992 under the Central Weather Bureau's project, entitled "Study of Precipitation Forecast over the Taiwan Area Using Limited Area Models." The objective of this project is to identify factors that are important to precipitation forecast over the Taiwan area using a limited area model. The TAMEX IOP#13 is used as the test-bed case for model sensitivity experiments utilizing both the CWB's Limited-Area Forecast Systems (RFS and MFS) and the NCAR/Penn State Mesoscale Model Version IV (MM4). A total of 7 numerical experiments using MM4 and 4 experiments using CWB models were performed in FY (fiscal year) 1991. These results were described in Kuo (1991), hereafter referred to as K1. The key conclusions of K1 can be summarized as following:

a. Systematic errors were identified in both the RFS and MFS in the prediction of the southward movement of the Mei-Yu front. These systematic errors were suspected to be related to the PBL parameterizations (RFS and MFS assume the bottom three levels to be well mixed, this might cause a significant weakening of the shallow cold air behind the Mei-Yu front).
b. Experiments with MM4 showed that precipitation forecast was highly sensitive to horizontal resolution. With 15 vertical levels, models with horizontal resolution of 45 km and 90 km were incapable of simulating heavy precipitation occurred during IOP#13, even though the movement of the Mei-Yu front was properly simulated.

c. The MM4 model with a grid resolution of 22.5 km simulated heavy precipitation over Taiwan, however, the timing was off by about 6 hours.

The objectives of the second year's research are: (1) to study the impact of vertical resolution, (2) to examine the sensitivity of rainfall forecast to precipitation parameterization, (3) to analyze all the model results, (4) to determine a control experiment, (5) to diagnose the results of the control experiment in an effort to understand the physical mechanisms associated with the heavy precipitation. A total of nine numerical experiments were performed using the MM4 model. The results of these experiments are described in this report. In collaboration with Dr. Kuo at NCAR, Dr. Glory Hsu at the Central Weather Bureau also conducted several experiments using the RFS and MFS. The results of these experiments were described in Hsu et al. (1992), and therefore not repeated here.

2. Experiment Design

Table 1 summarizes the numerical experiments performed using the MM4 model. The first three experiments all have 23 levels in the vertical, but with the horizontal resolution of 90 km, 45 km, and 22.5 km, respectively. These three experiments will be compared with the 15 level experiments conducted in FY-1991 at the same horizontal resolution to assess the impact of vertical resolution. The enhancement of vertical resolution occurs mostly in the upper and middle troposphere. The sigma distribution of the 15, and 23 levels are shown in Table 2. The CWB models use 12 vertical levels.

The second group of the experiments addresses the impact of precipitation parameterization. These experiments all use a horizontal grid resolution of 22.5 km and with 15 vertical levels. Experiment E22.5L15 uses the Kuo (1974) scheme for subgrid scale precipitation parameterization, while E22.5AS uses a modified Arakawa-Schubert (1974) scheme. Both experiments employ a simple nonconvective precipitation parameterization to treat the grid-resolvable scale rainfall (without explicit prediction of cloud water and rain water). Experiment E22.5GE uses the Grell (1992) scheme for subgrid scale precipitation and explicit moisture scheme (Hsie et al. 1984) for resolvable-scale precipitation. The explicit moisture scheme includes prognostic equations for cloud water and rain water with relevant microphysical processes. Both the modified Arakawa-Schubert scheme and the Grell scheme include convective downdraft parameterization.

To understand the impact of Taiwan's topography on the rainfall occurrence and distribution, we ran E45NT and E22.5NT with the terrain height of Taiwan set to 1 m, keeping every else within the domain the same as those of E45L15 and E22.5L15 (these two experiments were discussed in K1).

3. Results of Sensitivity Experiments

a. The impact of vertical resolution

Figure 1 shows the 36-h and 48-h prediction (valid at 0000 UTC and 1200 UTC 25 June 1987) of sea-level pressure and low-level (sigma = 0.97) wind fields of E90L23. Comparison of these forecasts with those of E90L15 shows that the position of the East China Sea

cyclone, the position of the Mei-Yu front, and the splitting of the Mei-Yu front as it encountered the Central Mountain Range (CMR) were nearly the same between these two experiments. The precipitation forecast of E90L23 is shown in Fig. 2. Again, the rainfall distribution was very similar to that of E90L15.

A comparison between E45L23 (Figures 3 and 4) and E45L15 yielded similar results in the vicinity of Taiwan. Again, the enhancement of vertical resolution (particularly in the upper-troposphere) did not make a significant impact on the low-level flow fields, the Mei-Yu front, and the related precipitation in the vicinity of Taiwan (Fig. 4). However, we note that at hour 36, the East China Sea cyclone was placed at 131°E, 29.5°N (a location better matched with the observation) in E45L23, while that in E45L15 it was located at 128°E, and 29°N. This cyclone was driven by an upper-level baroclinic wave (Yeh et al. 1990). An improved vertical resolution did improve the forecast for this cyclone.

With a faster eastward movement of the East China Sea cyclone in E45L23, the general synoptic scale setting in the vicinity of Taiwan was affected. Because E22.5L23 was driven by E45L23 in a one-way interactive mode, these effects caused some differences in the detailed mesoscale structure of pressure, wind and precipitation forecast between E22.5L23 and E22.5L15. We note that the surge of cold air along the southeastern China coast appeared to take place slightly earlier in the 23-L model (Fig. 5) as compared with that of the 15-L model (Fig. 7). By hour 48, the coastal ridging was slightly stronger in the 15-L model. Generally speaking, the differences in the pressure and wind distribution between these two experiments

were not significant. However, some subtle differences in the model precipitation forecast were noted. First, during the first 12-h period, the rainfall off the northwestern coast of Taiwan was slightly heavier in the 23-L model and with an orientation more consistent with the satellite observations. Second, significant precipitation was predicted off the Taichung coast between 0300 and 0600 UTC 25 June, which represents the second precipitation episodes associated with the IOP#13 (Jou and Deng 1990). Three hours later, heavy precipitation moved inland over Taichung. A similar sequence of events was also predicted by the 15-L model, except it was delayed by 3 hours (Fig. 8). A comparison with the satellite observations indicates that the timing of the 23-L model was more accurate, even though it still lagged behind the observation by approximately 3 hours.

In summary, we find that the effect of vertical resolution becomes increasingly important for models with higher horizontal resolution. This implies that for the CWB models with 90-km and 45-km resolution the impact of vertical resolution may not be as dramatic. However, as the CWB models use smaller grid size, an improvement in the vertical resolution will be important.

b. The impact of precipitation parameterization

The second group of sensitivity experiments examine the impact of precipitation parameterization on rainfall prediction. All the experiments use a horizontal grid size of 22.5 km with 15 vertical levels.

The use of the modified Arakawa-Schubert scheme produced a stronger East China Sea cyclone (994 mb versus 996 mb) at 0000 UTC 25 June (Figure 9a). The low-level wind field also indicates that

the cold air surge near the southeastern China coast moved faster southward (Figure 9b), in line with the observation. By 1200 UTC 25 June (Figure 9c), the mesoscale pressure distribution near the southeastern coast of China and in the vicinity of Taiwan was quite different from that of E22.5L15 (the Kuo scheme). The cold surge in E22.5AS near the China coast (Figure 9d) was not as well defined as that in E22.5L15 (the Kuo scheme) at this time. One possible reason for the more complicated mesoscale pressure distribution associated with the modified Arakawa-Schubert scheme might be related to the parameterized cumulus downdrafts. It is possible that the downdraft intensity (a tunable parameter in this scheme) was set too strong.

Substantial differences were found in the precipitation forecasts between these two experiments. During the first 12-h period (the first precipitation episode), most of the rainfall occurred to the north and northwest of Taiwan for both experiments. However, the rainfall amount was substantially larger for the experiment using the modified Arakawa-Schubert scheme (E22.5AS, Figure 10). For example, the maximum 3-h accumulated rainfall between 1800 UTC and 2100 UTC 24 June exceeded 25 mm in E22.5AS, while that in E22.5L15 was a little over 5 mm. During the 3-h period between 0000 UTC and 0300 UTC 25 June, E22.5AS produced a line of precipitation to the north of Taiwan, which was not found in E22.5L15 nor in the observation. The occurrence of the second precipitation episode started at 0600 UTC 25 June, similar to that of E22.5L15. However, the rainfall distribution was somewhat better than that of E22.5L15. Generally speaking, the use of the

modified Arakawa-Schubert scheme produced slightly improved precipitation forecast.

The use of the Grell (1992) subgrid-scale cumulus parameterization along with the explicit moisture scheme (E22.5GE) did not produce better forecast than either the Kuo scheme (E22.5L15) or the modified Arakawa-Schubert scheme (E22.5AS). Figure 11 shows the 12-h (valid at 0000 UTC 25 June) and 24-h (valid at 1200 UTC 25 June) forecast of sea-level pressure and surface wind for E22.5GE. Generally speaking, the pressure distribution in E22.5GE was more similar to that of the Kuo scheme than to the modified Arakawa-Schubert scheme. We note that the cold surge was fairly intense at 0000 UTC 25 June in E22.5GE. Northerly flow along the southeastern China coast reached as far south as 22.5°N. However, by 1200 UTC 25 June, the cold surge was cut off by a region of southerly flow immediately to the west of Taiwan. This rather unrealistic wind field distribution was not found in either the Kuo scheme or the modified Arakawa-Schubert scheme.

The precipitation forecast of E22.5GE (Figure 12) was also inferior to either the Kuo scheme or the modified Arakawa-Schubert scheme. The rainfall amount in E22.5GE was the lowest among the three experiments. During the first 12-h period rainfall in the vicinity of Taiwan rarely exceeded 5 mm, while in the second 12-h period, only a few isolated points over the west coast of Taiwan predicted rainfall more than 5 mm.

These experiments clearly indicate that the mesoscale prediction of pressure, wind and precipitation distribution is highly sensitive to precipitation parameterization. Without further

experimentation of these schemes on a large number of cases, and without in-depth analysis of the performance of each scheme, it is not possible to conclude one scheme being definitely better than the other. Although, based on the testing performed up to this point, the Kuo scheme appears to be quite adequate for the simulation of the IOP#13 case. It is also possible that with further adjustment and tuning, the performance of the modified Arakawa-Schubert scheme and the Grell scheme can be substantially improved (for example, adjusting the downdraft intensity).

c. The effects of orography

In an effort to understand the impact of the Central Mountain Range (CMR) on the Mei-Yu front and its associated precipitation distribution, we performed Exps. E45NT and E22.5NT. In both experiments we set the terrain height of Taiwan to 1 m, while keeping everything else the same. The main purpose of E45NT was to provide lateral boundary conditions for E22.5NT. Since the orography of Taiwan was of a scale of 100 km x 300 km, the impact of orography can be much better revealed in the 22.5 km model. Therefore, our discussion will focus on the results of E22.5NT.

Figure 13 shows the sea-level pressure and surface winds valid at 0000 UTC and 1200 UTC 25 June as predicted by E22.5NT. Without the orography of Taiwan, significant changes were found in the mesoscale pressure distribution and the surface wind field. First of the all, the mesoscale pressure ridge on the upwind side of the Central Mountain Range no longer existed in the no-terrain experiment. The coastal ridging along the southeastern China coast was still reproduced by the E22.5NT experiment. This is to be

expected because no modification was made to the orography of China.

The split and deformation of the Mei-Yu front found in E22.5L15, as revealed by the surface wind field, was missing in the no-terrain experiment. Instead, a continuous shear line associated with the Mei-Yu front was predicted at 0000 UTC 25 June. By 1200 UTC 25, an arc shaped Mei-Yu front was predicted to the west of Taiwan in the no-terrain experiment. This is due to the enhanced cold air damming along the China coast.

We note that the Mei-Yu front moved slightly slower over Taiwan than over the Pacific ocean. As a result, by 1200 UTC 25 June, a slight frontal deformation was found along the east coast of Taiwan. This was due to the differences in friction between land and ocean. It is important to recognize that even though the terrain height was reduced, Taiwan was still represented as a land mass. A comparison of this simulation and the E22.5L15 simulation shows that the frontal deformation caused by differential frictional effects was significantly weaker than that caused by orography.

To illustrate further the impact of orography we compare the the temperature field at σ = 0.97 for both experiments in Figure 14. A major difference in the variation of frontal intensity was found between these two experiments. In the control experiment with the CMR, the temperature gradient was very large, 8°C $(100\ km)^{-1}$, for the western segment of the Mei-Yu front (between Taiwan and the coast of China). In sharp contrast, the temperature gradient was about 2°C $(100\ km)^{-1}$ in the eastern segment (to the east of Taiwan). In the no-terrain experiment, the temperature gradient was much

more homogeneous in the vicinity of Taiwan, ~2.5°C (100 km)$^{-1}$, except for the portion along the coast of China, where cold air damming enhanced the frontal gradient. These differences show that the effect of CMR was not only to deform the Mei-Yu front, but also to block the southwesterly monsoon flow on the western side of Taiwan. As a result the warm, moist monsoon air was brought directly against the colder, drier air behind Mei-Yu front, causing substantially enhanced frontal gradient to the west of Taiwan. On the contrary, the faster movement of the cold air along the eastern side of CMR spread the cold air over a longer distance. Consequently, the temperature gradient to the east of Taiwan was slightly weakened as compared with the no-terrain experiment.

Figure 15 shows the corresponding equivalent temperature fields for these two experiments. In addition to differences in frontal gradient discussed earlier, a pocket of relatively low θ_e air was found over southeastern coast of Taiwan in the control experiment (E22.5L15). This feature was not found in the no-terrain experiment. From previous modeling studies utilizing MM4 on the TAMEX meso-low cases, that this was found to be a consequence of flow blocking by the CMR. As the southwesterly monsoon air was blocked by the CMR, low θ_e air in the mid-troposphere descended into the lower troposphere at the lee of the CMR. It should be commented that a meso-low was observed in the TAMEX IOP#13 case over southeastern coast of Taiwan. This is consistent with the model simulation presented here.

The precipitation distribution (Figure 16) was strongly affected by the CMR. When the CMR was removed (E22.5NT), the Mei-Yu

rainband cut through Taiwan with little modification. Three-hour rainfall exceeding 5 mm was predicted over the northern half of Taiwan between 1500 UTC and 1800 UTC 24 June, which did not occur in the control experiment. Also, a band of precipitation exceeding 10 mm $(3h)^{-1}$ was predicted to cover central Taiwan during the 3-h period ending at 0900 UTC 25 June. In contrast, significant precipitation was predicted in the control experiment along the west coast of Taiwan with a much higher intensity. For example, nearly 40 mm of rain was predicted over Taichung in the 3-h period ending at 1200 UTC 25 June, which was not found in the no-terrain experiment.

In summary, we found that the Central Mountain Range produced significant alteration of the Mei-Yu front, blocked the southwesterly monsoon flow and was responsible for the mesoscale precipitation distribution. To fully realize the impact of Taiwan's orography on weather systems over the region, a model with a resolution on the order of 20 km is needed.

d. Nonhydrostatic model simulation

The NCAR mesoscale modeling group recently developed a nonhydrostatic version of MM4 which can be used for real data simulation and prediction (Dudhia 1992). It is of interest to examine the usefulness of this model in the simulation of the TAMEX IOP#13. For this purpose we performed a 22.5-km 23 level nonhydrostatic (NH) model integration (E22.3NH) with the same physical parameterizations as those of E22.5L23. At a horizontal grid length of 22.5 km, we do not expect the nonhydrostatic effects to be important. However, because the NH model includes predictive

equation for pressure perturbation at each vertical level, the pressure gradient force can be calculated much more accurately (the usual pressure gradient force problems in sigma coordinate models no longer exist).

Figure 17 shows the sea-level pressure and surface wind forecasts of E22.5NH verifying at 0000 UTC and 1200 UTC 25 June. Generally speaking, the results of E22.5NH are similar to those of E22.5L23. However, we note a few subtle differences. First, the cold air damming along the southeastern coast of China appears to be better simulated. A pressure trough (inverted trough) was located over the Taiwan Strait, immediately to the east of the mesoscale pressure ridge associated with the cold air damming. Most interestingly, we see a meso-low over the Taiwan Strait at 0000 UTC 25 June, off the coast of Hsin-Chu, a location climatologically favored for meso-low formation. At 1200 UTC, another meso-low was predicted off the southeastern coast of Taiwan. Neither of these two meso-lows were clearly visible in the hydrostatic simulation of E22.5L23.

The surface wind field indicates that the wind speed was stronger along the southeastern coast of China and off the southeastern coast of Taiwan in the nonhydrostatic simulation. These results are consistent with the strong cold surge along the China coast and the development of meso-lows.

The precipitation distribution (Figure 18) predicted by E22.5NH was very similar to that of E22.5L23, except the precipitation amount was larger for the NH model. The NH model predicted rainfall amount

exceeding 30 mm in several 3-h periods, which was consistent with the observed rainfall intensity.

Although the use of nonhydrostatic model with a 22.5-km grid did not produce dramatic differences from those of the hydrostatic model, we do note general improvements in the simulation. Perhaps, the two most significant implications are: (1) it is feasible to perform nonhydrostatic numerical weather prediction over Taiwan, and (2) with a nonhydrostatic model a much higher horizontal resolution can be used for numerical simulation and operational forecasts.

4. Model diagnosis

An important scientific question concerning the TAMEX IOP#13 is the physical mechanisms responsible for the occurrence of heavy rainfall. With a successful model simulation, detailed diagnosis can be performed to gain insight into these physical processes. As discussed in K1, the E22.5L15 experiment simulated the deformation of the Mei-Yu front, the cold air damming along the coasts of China and Taiwan, and the heavy precipitation over Taiwan very well, although the timing was off by approximately 6 hours. Although the model simulation was not perfect, it is believed that the model reproduced the physical processes involved in this event reasonably well. If allowance is made for differences in timing, the model results can provide valuable information on the physical mechanisms associated with this heavy rainfall event. In this section, we show some of the model diagnoses based on the results of E22.5L15.

A total of three vertical cross sections were taken, one along the southeastern coast of China, the second along the west coast of

Taiwan, and third cutting across the Taiwan Strait and the Central Mountain Range. The position of these cross sections are shown in Figure 7. Figure 19 shows the cross section of horizontal wind, relative humidity, θ_e and vertical circulations along the coast of China at 12 h intervals. The horizontal wind show northerly and northeasterly behind the front, and southerly and southwesterly ahead (and above) the front. The cold air moved very rapidly along the China coast, with a displacement of about 150 km in 12 h. The southwesterly flow above the front was moist, with relative humidity exceeding 90%.

There were considerable differences in the θ_e field across the front, with θ_e exceeding 370 K in the prefrontal boundary layer, and θ_e below 340 K in the postfrontal air. The front was very shallow as revealed both in the horizontal wind field and the θ_e field. The depth of the cold air increased slowly from the surface to about 1500 m over a 500 km distance (as shown in the cross section at 1200 UTC 25 June). The shallowness of the cold air might explain the difficulties of the CWB models in handling the frontal interaction with topography if the lowest three layers are well-mixed and (or) the models have relatively low vertical resolution. The cross section also shows a direct circulation across the front, with warm air rising ahead and above the front and cold air sinking behind the front.

The cross section along the west coast of Taiwan (Figure 20) shows many differences from that of the southeastern coast of China. The front moved about 100 km during the first 12 hours, and about another 50 km in the next 12 hours. This is consistent with the observation of enhanced southward advancement of cold air along

the China coast and quasi-stagnation along the west coast of Taiwan. It should be commented that the front had an east-west orientation prior to its encounter with the orography of Taiwan.

The same kind of thermally direct vertical circulation associated with the Mei-Yu front was also found in the cross section along the west coast of Taiwan. The humidity was also high above and ahead of the front. Most interestingly, at 1200 UTC 25 June, the cross section cut through the region of heavy precipitation. A column of saturated air with strong vertical velocity was located at the middle of the cross section. The heavy precipitation occurred ahead of the Mei-Yu front by approximately 100 km. This precipitation system was rooted within the boundary layer θ_e of 370 K, and occurred entirely within the southwesterly monsoon air. This is consistent with the pre-frontal squall line observed by Doppler radars in this case.

To understand better the environment of the squall line we show in Figure 21 the cross section cutting through the Taiwan Strait and the Central Mountain Range at 1200 UTC 25 June. The cross section shows that the heavy precipitation took place on the upwind side of the Central Mountain Range, ahead of (and to the southeast of) the Mei-Yu front. From Figure 20 and 21, we can visualize that as the Mei-Yu front advanced southward, the warm, moist southwesterly monsoon air was squeezed by the cold air to the north and the Central Mountain Range to the east, and was forced to rise on the upwind side of the mountain, causing heavy precipitation. If the Central Mountain Range were not there, then the monsoon air would just flow eastward without enhanced lifting. Thus, the precipitation

would be mainly produced by frontal lifting, and the precipitation amount would be considerably less. This conceptual model is consistent with the results of the no-mountain experiment, E22.5NT.

5. Summary and Conclusions

During the past year, we performed a total of nine experiments using the NCAR/Penn State mesoscale model MM4, with an interest to examine factors important to heavy precipitation forecasts using a limited-area model. The key results can be summarized as follows:

1. Increase the vertical resolution from 15 levels to 23 levels had little impact on the results of 90-km, 45-km and 22.5-km models. The main reason for the lack of impact was due to the fact that most of the increase in vertical resolution took place in the middle and upper troposphere. For the simulation of the TAMEX IOP#13, it was the low-level frontal forcing and its interaction with the topography that was crucial for heavy precipitation. The increased vertical resolution, though improved the simulation of upper-level systems, had no significant impact on the forecast in the vicinity of Taiwan. The impact of vertical resolution, though not large, increased with increased horizontal resolution. With finer horizontal resolution, more precipitation occurs on the grid-resolvable scale. The increased vertical resolution will influence the development of grid point saturation and resolvable scale precipitation. For numerical weather prediction over Taiwan, an improvement in horizontal resolution from 45-km to a grid size of at least 22.5 km is crucial. The improvement in vertical

resolution is not as important. We recommend adding a few levels in the lower troposphere for the CWB models.

2. Test of different precipitation parameterizations on a 22.5 km model revealed considerable forecast sensitivity. Not only the precipitation amount and precipitation distribution were affected, the mesoscale pressure and wind fields were also affected. Among the three precipitation parameterizations tested, the Kuo scheme coupled with a simple nonconvective precipitation parameterization produced the best pressure and wind field distribution, while the Arakawa-Schubert scheme produced better precipitation distribution and amount. The Grell scheme combined with the more sophisticated explicit moisture scheme gave the worst results. Although the Kuo-scheme appears to be quite adequate for this case, it is possible that further tuning of the Arakawa-Schubert scheme and the Grell scheme can improve their performance. Considerably more testing is required before a definite conclusion can be given.
3. The removal of the Taiwan's orography produced significant changes on the model simulation. A comparison of experiments with and without the orography of Taiwan indicates that the effect of the Central Mountain Range was to: (1) split the Mei-Yu front into eastern and western sections, (2) block the low-level southwesterly monsoon flow, (3) cause the middle-level low θ_e air to descend to the lee of the Central Mountain Range, (4) enhance the temperature and θ_e gradient of the Mei-Yu front to the west of Taiwan, and (5) produce enhanced

precipitation on the upwind side of the mountain by blocking and lifting the warm, moist monsoon air. The importance of the CMR on the flow field, pressure field and precipitation distribution again calls for the use of high resolution models for numerical weather prediction in Taiwan. Only with high horizontal resolution can the CMR be properly represented in the model.

4. The use of nonhydrostatic mesoscale model at a horizontal resolution of 22.5 km produced moderate improvement in the model simulation. The cold air damming along the China coast and the meso-lows located off the northwestern coast and southeastern coast of Taiwan were all simulated with improved accuracy. Also, the precipitation amount produced by the nonhydrostatic model was closer to the observed amount. More significantly, our results indicate that it is feasible to use nonhydrostatic mesoscale model for numerical weather prediction in Taiwan.
5. Detailed model diagnoses were performed on the results of E22.5L15 experiment. Vertical cross sections perpendicular to the front indicates extreme shallowness of the cold air behind the Mei-Yu front. The frontal slope was about 0.3/100. The shallowness of the cold air might explain the difficulties encountered by CWB's RFS and MFS in the simulation of the Mei-Yu front and its movement, in particular if the lowest three-levels were assumed to be well-mixed. The model diagnosis also indicates thermally direct secondary circulation across the Mei-Yu front. The heavy precipitation was found to

take place within the warm, moist southwesterly monsoon flow, approximately 100 km ahead of the front. The model results suggest that as the Mei-Yu front advanced southward, the warm, moist monsoon air was forced to rise over west central Taiwan (near Taichung), as it was blocked by the Central Mountain Range to the east and the cold air to the north. The pre-frontal nature of the simulated heavy precipitation was consistent with the Doppler radar observation of the TAMEX IOP#13 pre-frontal squall line.

Acknowledgement

I thank Dr. Yueh-Jiuan Hsu for performing the RFS and MFS experiments and Ms. Wei Wang for performing the MM4 experiments and diagnoses. I am also grateful to Drs. Simon Chang, Ming-Dean Cheng and Melinda Peng for fruitful discussions.

Table 1. Numerical experiments performed using the NCAR/Penn State mesoscale model MM4.

Exp. Name	Grid Size	Vertical Level	Precip. Physics	Remarks
E90L23	90 km	23	Kuo	23 level experiment
E45L23	45 km	23	Kuo	23 level experiment
E22.5L23	22.5 km	23	Kuo	23 level experiment
E22.5L15	22.5 km	15	Kuo	control experiment
E22.5AS	22.5 km	15	A.-S.	Arakawa-Schubert
E22.5GE	22.5 km	15	Grell	with explicit scheme
E45NT	45 km	15	Kuo	No Terrain
E22.5NT	22.5 km	15	Kuo	No Terrain
E22.5NH	22.5 km	23	Kuo	Nonhydrostatic model

Table 2. Sigma distribution for 12, 15, and 23 level models.

23 Levels:
1., .99, .98, .96, .93, .89, .85, .8, .75, .7, .65, .6,
.55, .5, .45, .4, .35, .3, .25, .2, .15, .1, 0.05, 0.0

15 Levels:
1., .99, .98, .96, .93, .89, .84, .78, .7, .6, .5, .4, .3, .2, .1, 0.0

12 Levels:
1., .95, .90, .80, .7, .6, .5, .4, .3, .2, .1, .05, 0.0

References

Arakawa, A., and W. H. Schubert, 1974: Interaction of a cumulus cloud ensemble with the large-scale environment. Part I. *J. Atmos. Sci.*, **31**, 674-701.

Dudhia, J., 1992: A nonhydrostatic version of the Penn State/NCAR mesoscale model. *Mon. Wea. Rev.*, (in press).

Grell, G. A., 1992: Prognostic evaluation of assumptions used by cumulus parameterizations. *Mon. Wea. Rev.*, (in press).

Hsie, E.-Y., R. A. Anthes, D. Keyser, 1984: Numerical simulation of frontogenesis in a moist atmosphere. *J. Atmos. Sci.*, **41**, 2581-2594.

Hsu, Y.-J. G., Y.-H. Kuo, and W. Wang, 1991: Prediction of a heavy rainfall event over Taiwan. Preprints, *Ninth Conference on Numerical Weather Prediction*, 14-18 October 1991, Denver, Colorado, 786-789.

_____, _____, and S. Chang, 1992: Numerical simulation of TAMEX IOP#13 using the CWB Limited-Area Forecast Systems. Proceedings, *Conference on Weather Analysis and Forecasting*, 23-25 April, 1992, Taipei, 11-15.

Kuo, H. L., 1974: Further studies of the parameterization of the influence of cumulus convection on large-scale flow. *J. Atmos. Sci.*, **31**, 1232-1240.

Kuo, Y.-H., 1991: Prediction of a heavy rainfall event over Taiwan using limited-area models. Report submitted to Central Weather Bureau, 21 June 1991.

Jou, B. J.-D., S.-M. Deng, 1990: Mesoscale characteristics of Mei-Yu front. Proceedings, *Workshop on TAMEX Scientific Results*, 24-26 September 1990, Boulder, CO, 150-157.

Yeh, C.-C., P.-L. Lin, and S.-Y. Chou, 1990: On the synoptic weather condition associated with a mesoscale convective system in TAMEX IOP-13. Proceedings, *Weather Analysis and Forecasting*, 3-5 May 1990, Taipei, 95-106.

Figure Captions

Fig. 1. Sea-level pressure and σ = 0.995 wind for (a), (b) 36-h, (c), (d) 48-h forecasts of E90L23 verifying at 0000 UTC 25 and 1200 25 June 1987, respectively.

Fig. 2. 24-h accumulated rainfall ending at 1200 UTC 25 June 1987 for E90L23.

Fig. 3. Sea-level pressure and σ = 0.995 wind for (a), (b) 36-h, (c), (d) 48-h forecasts of E45L23 verifying at 0000 UTC 25 and 1200 25 June 1987, respectively.

Fig. 4. 24-h accumulated rainfall ending at 1200 UTC 25 June 1987 for E45L23.

Fig. 5. Sea-level pressure and σ = 0.995 wind for (a), (b) 12-h, (c), (d) 24-h forecasts of E22.5L23 verifying at 0000 UTC 25 and 1200 25 June 1987, respectively.

Fig. 6. 3-h accumulated total rainfall at 3-h intervals for E22.5L23 ending at (a) 1200 UTC 24, (b) 1800 UTC 24, (c) 2100 UTC 24, (d) 0000 UTC 25, (e) 0300 UTC 25, (f) 0600 UTC 25, (g) 0900 UTC 25, and (h) 1200 UTC 25 June 1987.

Fig. 7. Sea-level pressure and σ = 0.995 wind for (a), (b) 12-h, (c), (d) 24-h forecasts of E22.5L15 (the Kuo scheme) verifying at 0000 UTC 25 and 1200 25 June 1987, respectively.

Fig. 8. 3-h accumulated total rainfall at 3-h intervals for E22.5L15 (the Kuo scheme) ending at (a) 1200 UTC 24, (b) 1800 UTC 24, (c) 2100 UTC 24, (d) 0000 UTC 25, (e) 0300 UTC 25, (f) 0600 UTC 25, (g) 0900 UTC 25, and (h) 1200 UTC 25 June 1987.

Fig. 9. Sea-level pressure and σ = 0.995 wind for (a), (b) 12-h, (c), (d) 24-h forecasts of E22.5AS (the Arakawa-Schubert scheme) verifying at 0000 UTC 25 and 1200 25 June 1987, respectively.

Fig. 10. 3-h accumulated total rainfall at 3-h intervals for E22.5AS (the Arakawa-Schubert scheme) ending at (a) 1200 UTC 24, (b) 1800 UTC 24, (c) 2100 UTC 24, (d) 0000 UTC 25, (e) 0300 UTC 25, (f) 0600 UTC 25, (g) 0900 UTC 25, and (h) 1200 UTC 25 June 1987.

Fig. 11. Sea-level pressure and σ = 0.995 wind for (a), (b) 12-h, (c), (d) 24-h forecasts of E22.5GE (the Grell + Explicit scheme) verifying at 0000 UTC 25 and 1200 25 June 1987, respectively.

Fig. 12. 3-h accumulated total rainfall at 3-h intervals for E22.5GE (the Grell + Explicit scheme) ending at (a) 1200 UTC 24, (b) 1800 UTC 24, (c) 2100 UTC 24, (d) 0000 UTC 25, (e) 0300 UTC 25, (f) 0600 UTC 25, (g) 0900 UTC 25, and (h) 1200 UTC 25 June 1987.

Fig. 13. Sea-level pressure and σ = 0.995 wind for (a), (b) 12-h, (c), (d) 24-h forecasts of E22.5NT verifying at 0000 UTC 25 and 1200 25 June 1987, respectively.

Fig. 14. Temperature at σ = 0.97 for (a) E22.5L15 and (b) E22.5NT experiments verifying at 0000 UTC 25 June.

Fig. 15. Equivalent potential temperature at σ = 0.97 for (a) E22.5L15 and (b) E22.5NT experiments verifying at 0000 UTC 25 June.

Fig. 16. 3-h accumulated total rainfall at 3-h intervals for E22.5NT ending at (a) 1200 UTC 24, (b) 1800 UTC 24, (c) 2100 UTC 24, (d) 0000 UTC 25, (e) 0300 UTC 25, (f) 0600 UTC 25, (g) 0900 UTC 25, and (h) 1200 UTC 25 June 1987.

Fig. 17. Sea-level pressure and σ = 0.995 wind for (a), (b) 12-h, (c), (d) 24-h forecasts of E22.5NH verifying at 0000 UTC 25 and 1200 25 June 1987, respectively.

Fig. 18. 3-h accumulated total rainfall at 3-h intervals for E22.5NH ending at (a) 1200 UTC 24, (b) 1800 UTC 24, (c) 2100 UTC 24, (d) 0000 UTC 25, (e) 0300 UTC 25, (f) 0600 UTC 25, (g) 0900 UTC 25, and (h) 1200 UTC 25 June 1987.

Fig. 19. Cross section of horizontal wind and relative humidity (upper panels) and equivalent potential temperature and vertical circulations (lower panels) of E22.5L15 for the cross section AB (along the coast of China, shown in Fig. 7) verifying at (a) 1200 UTC 24, (b) 0000 UTC 25, and (c) 1200 UTC 25 June.

Fig. 20. Cross section of horizontal wind and relative humidity (upper panels) and equivalent potential temperature and vertical circulations (lower panels) of E22.5L15 for the cross section CD (along the west coast of Taiwan, shown in Fig. 7) verifying at (a) 1200 UTC 24, (b) 0000 UTC 25, and (c) 1200 UTC 25 June.

Fig. 21. Cross section of (a) horizontal wind and relative humidity and (b) equivalent potential temperature and vertical circulations of E22.5L15 for the cross section EF (cutting through the Taiwan Strait and the Central Mountain Range as shown in Fig. 7) verifying 1200 UTC 25 June.

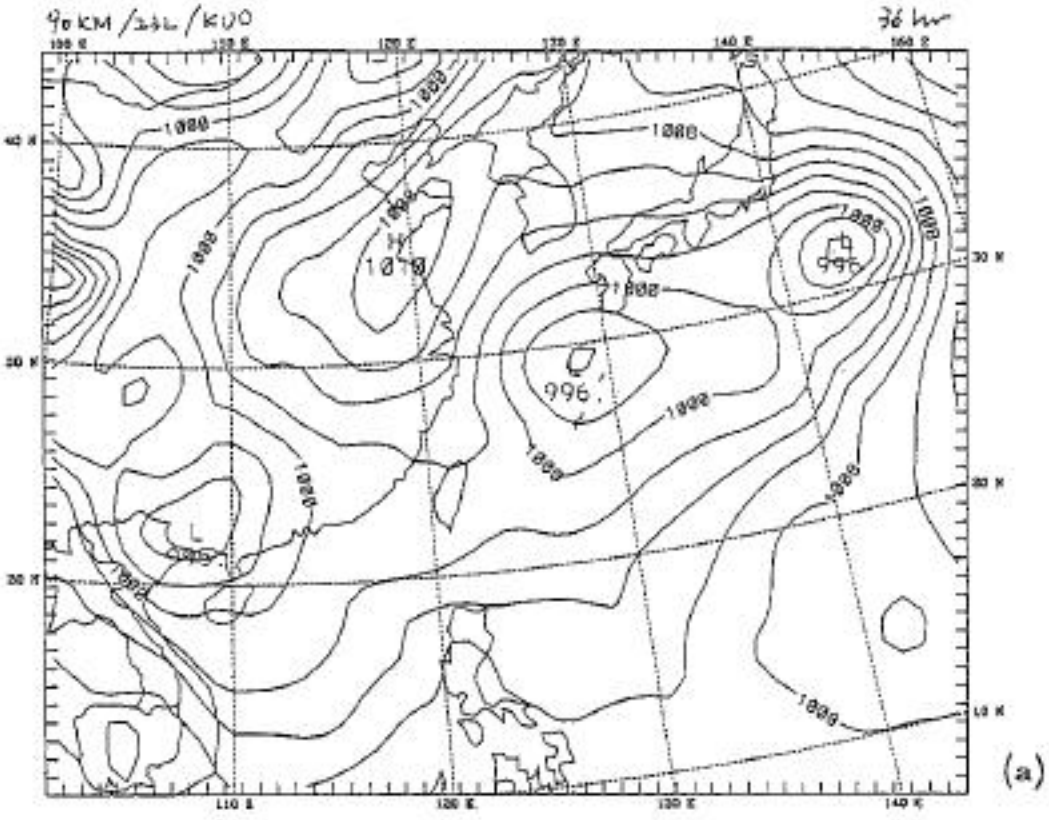
90KM/24L/KUO
36 hr
1010
996
1000
1004
1008
1012
1016
1020
110 E
120 E
130 E
140 E
40 N
30 N
20 N

(a)

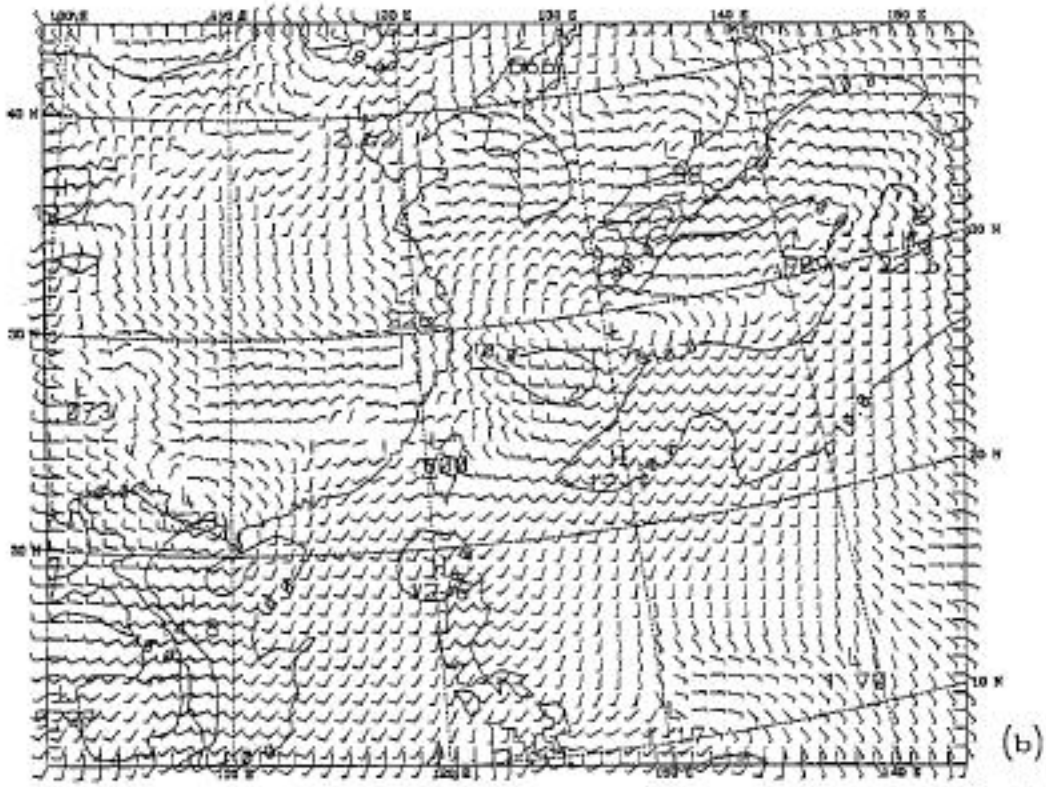

(b)

Fig. 1

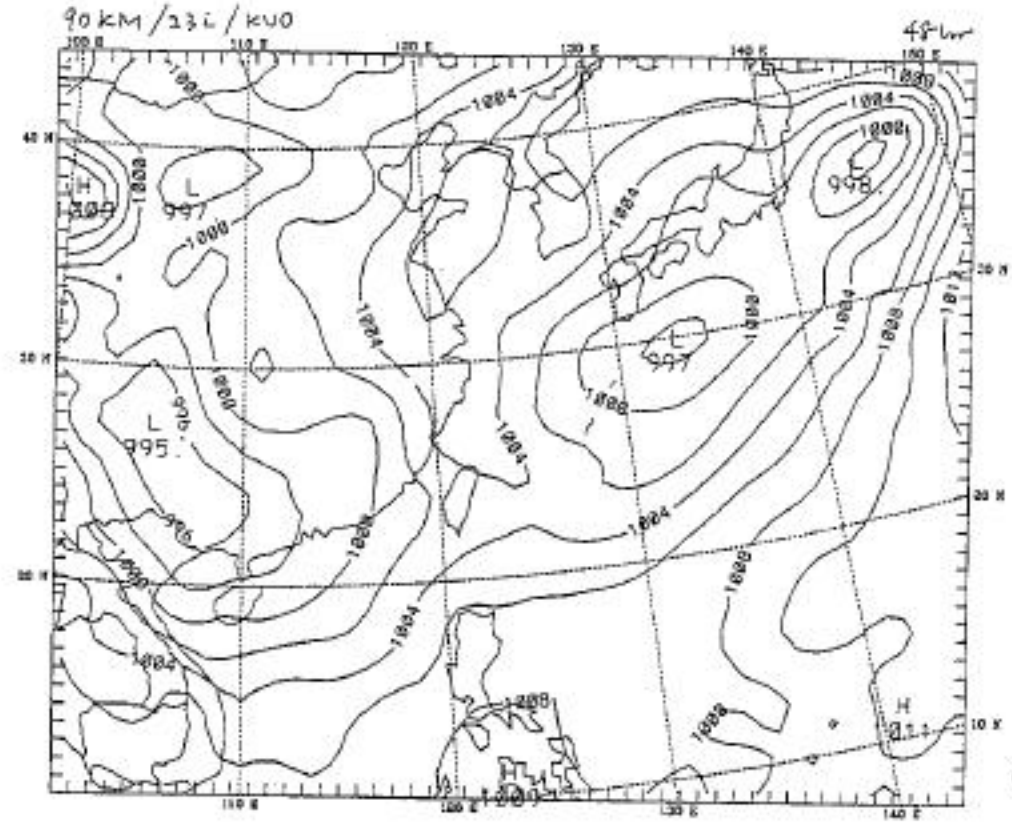

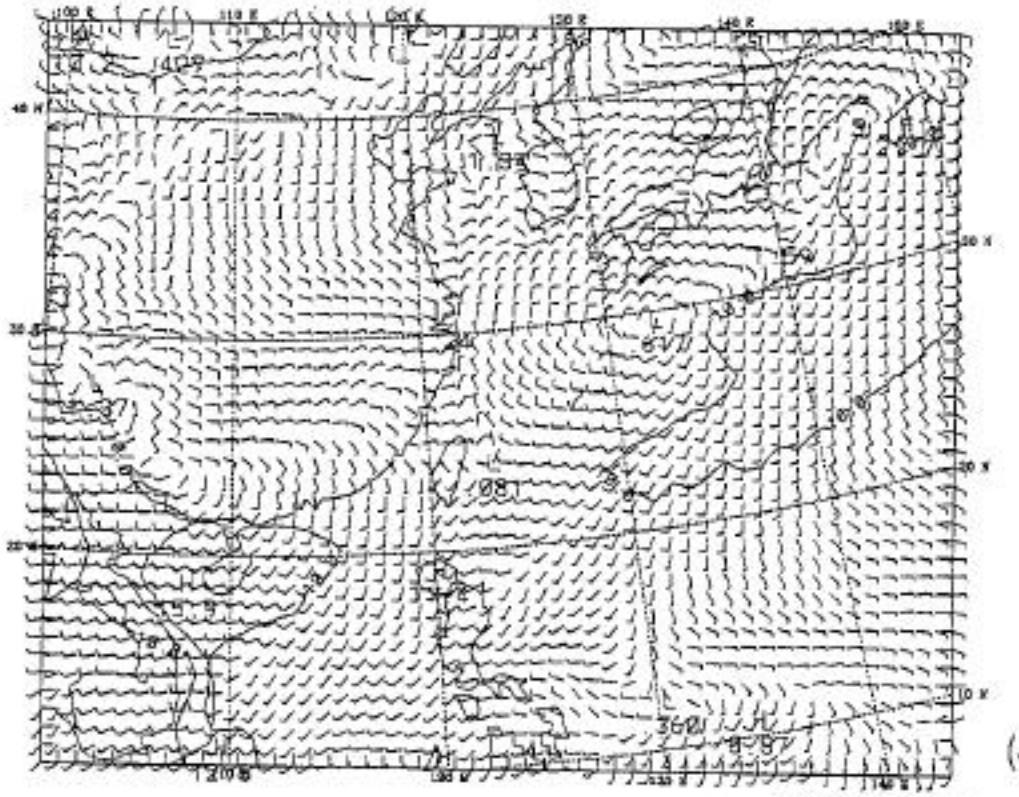

Fig. 1 Continued

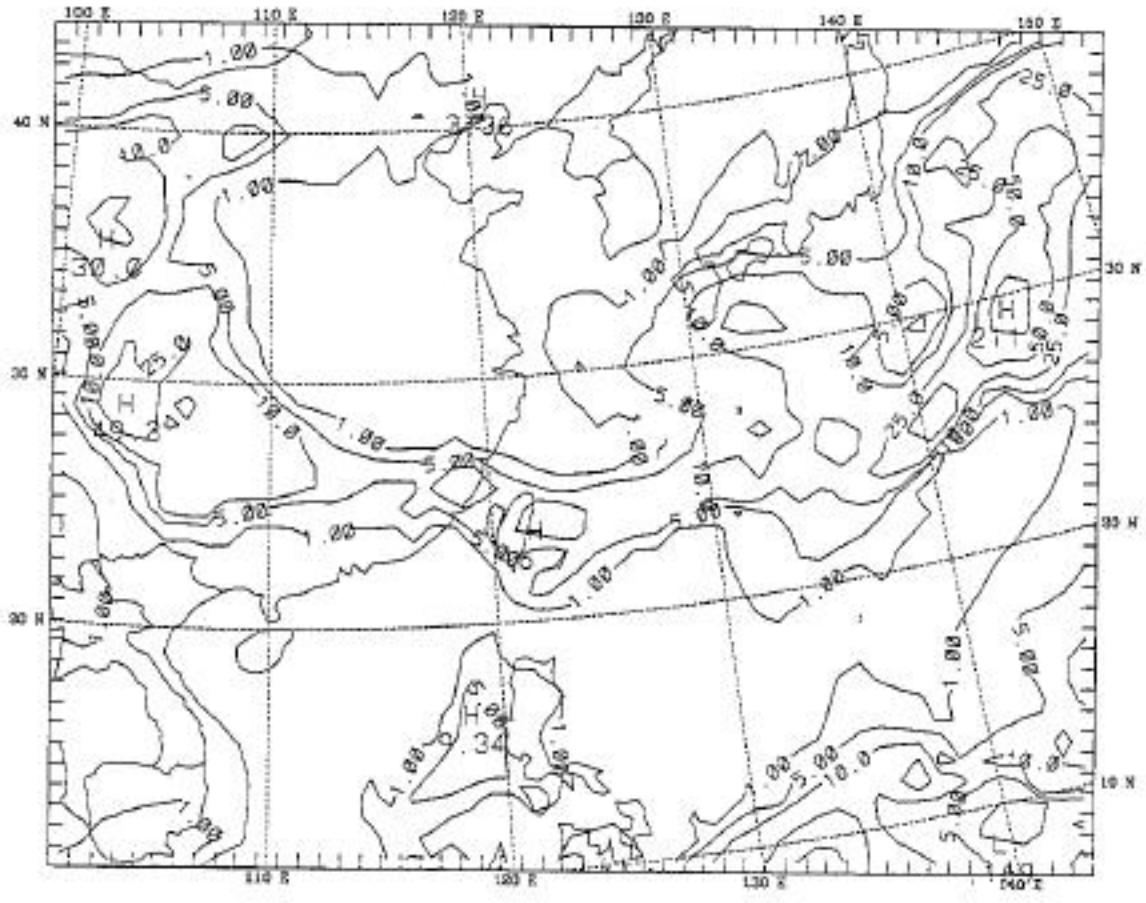
SIGMA =1.000 TEND RNT ( ) 87062312+ 48.00h SMOOTH= 0
100 E
110 E
120 E
130 E
140 E
150 E
40 N
30 N
20 N
10 N
IOP13 90KM 23L (Kuo, HIRPBL)
CONTOUR FROM 0.0000 TO 0.0000 CONTOUR INTERVAL OF 5.0000

Fig. 2

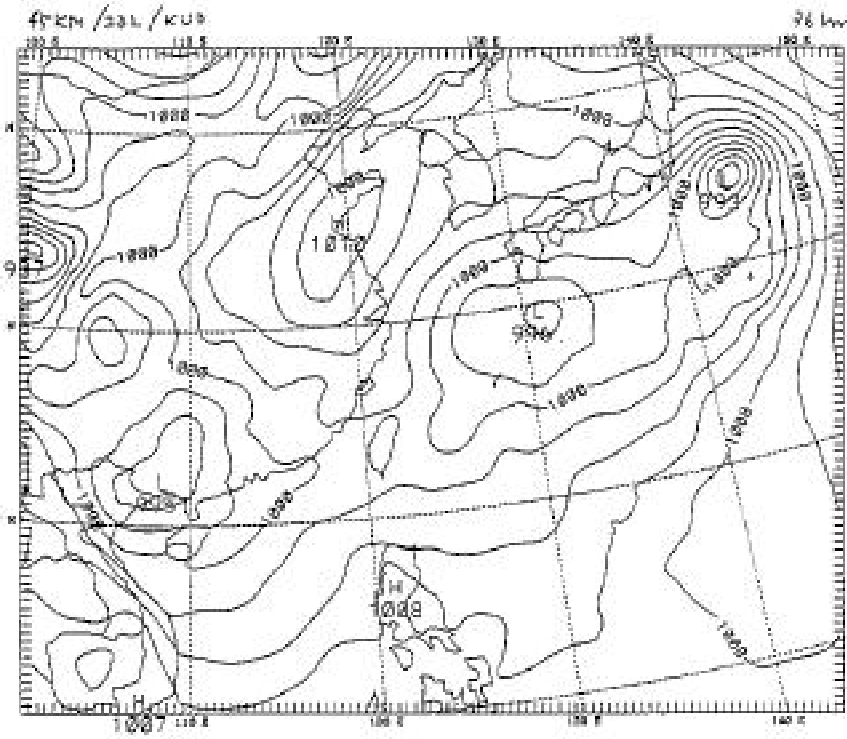

(a)

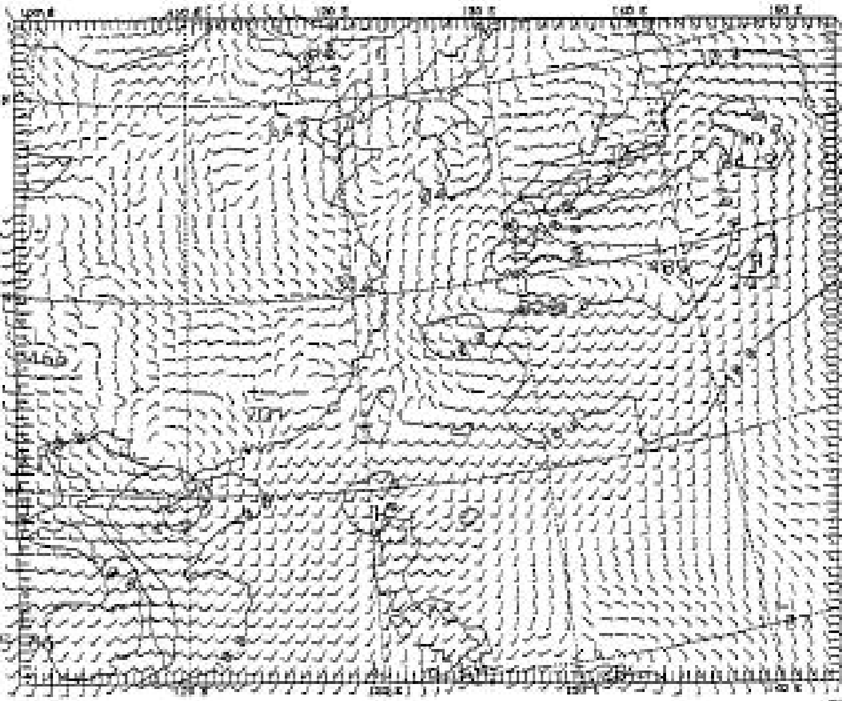

(b)

Fig. 3

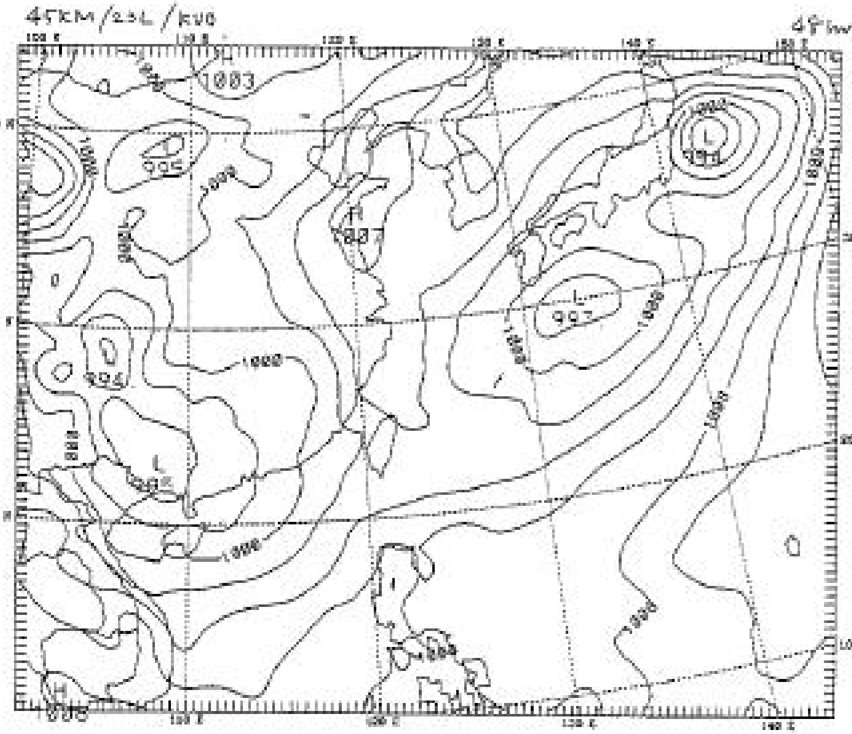

(c)

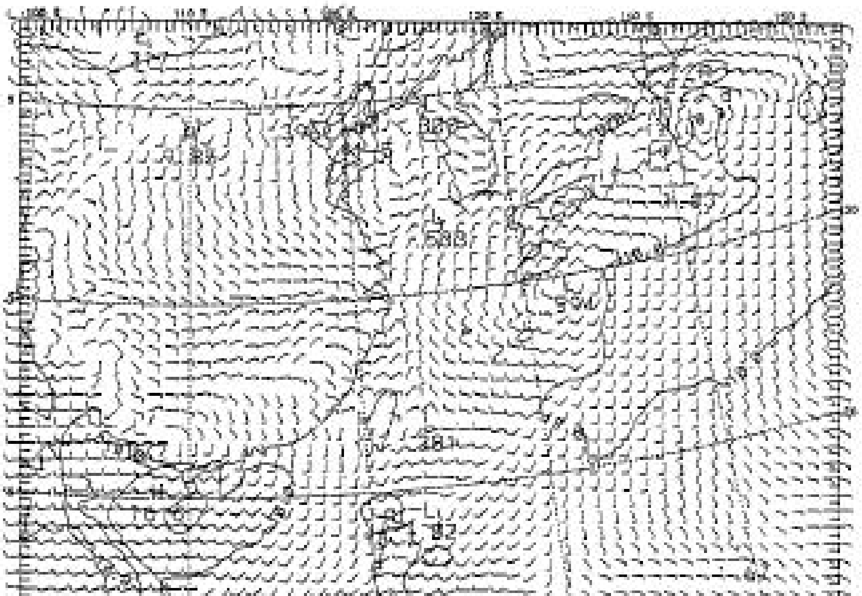

(d)

Fig. 3 Continued

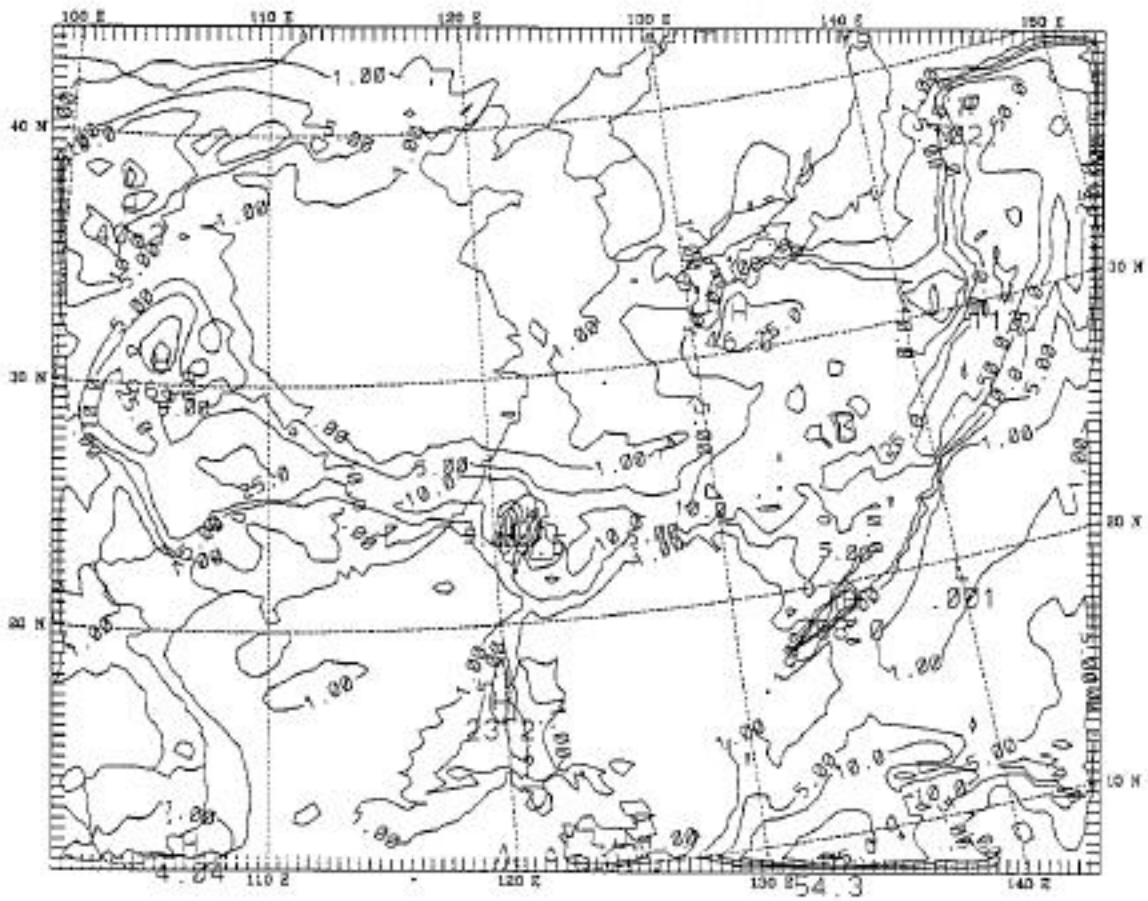
SIGMA =1.000 TEND RNT ( ) 87062312+ 48.00h SMOOTH= 0
100 E
110 E
120 E
130 E
140 E
150 E
40 N
30 N
20 N
10 N
1.00
5.00
10.00
54.3
TOP13 45KM 23L (Kuo, HIRPBL)
CONTOUR FROM 000000 TO 000000 CONTOUR INTERVAL OF 5.0000

Fig. 4

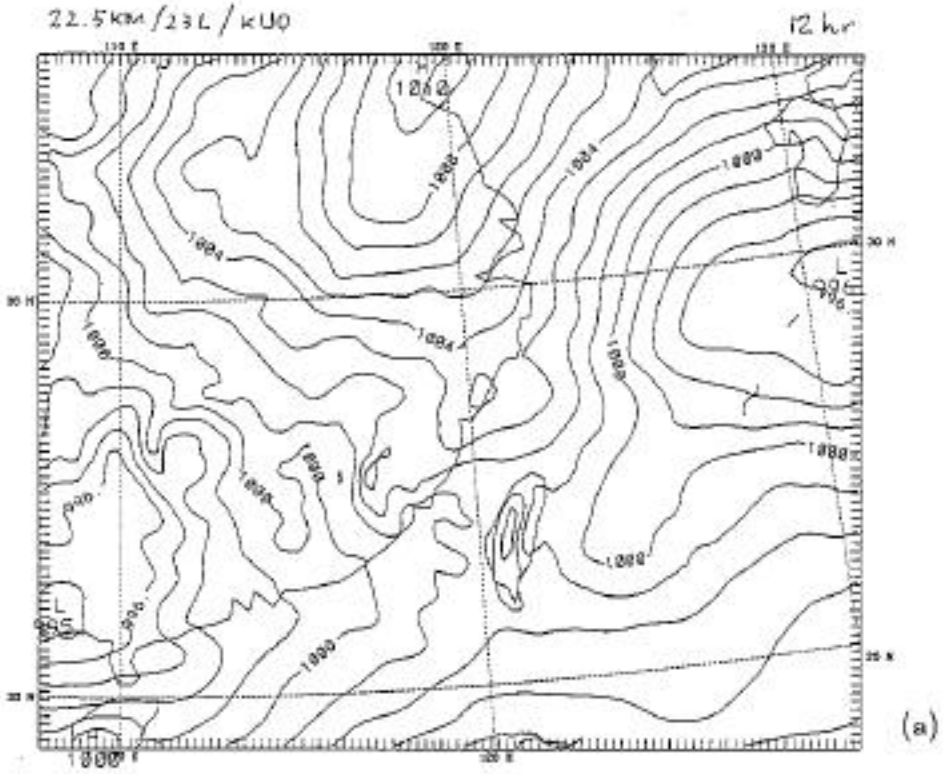

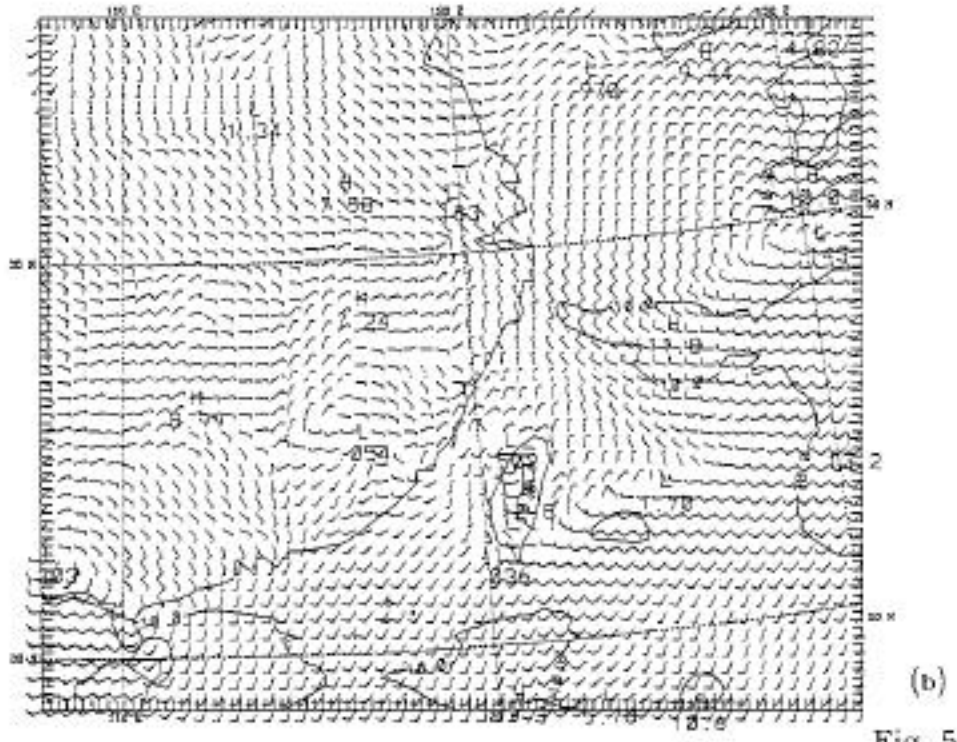

Fig. 5

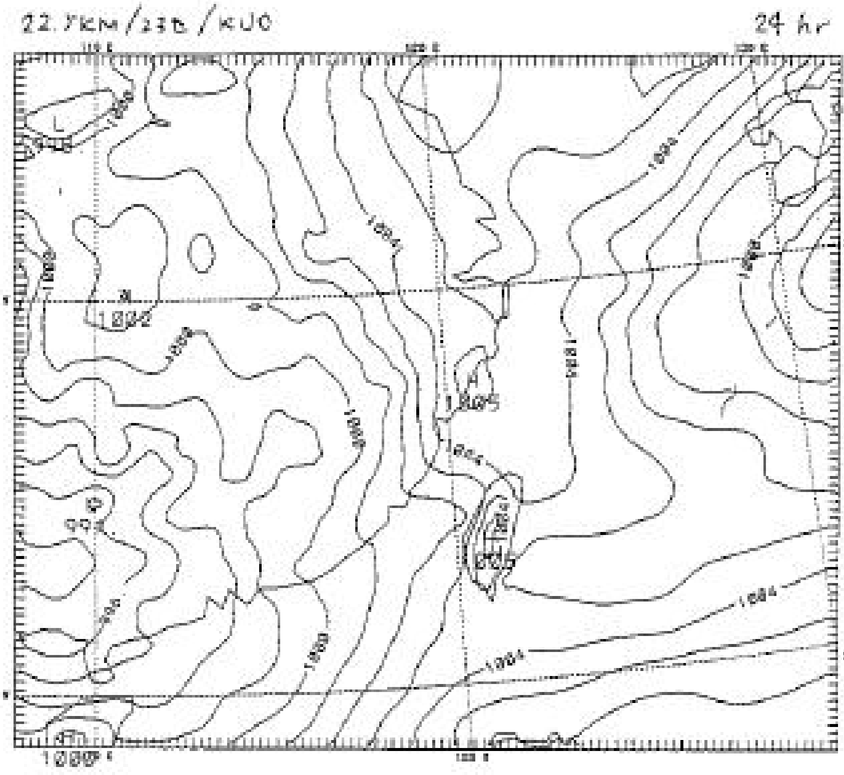

(c)

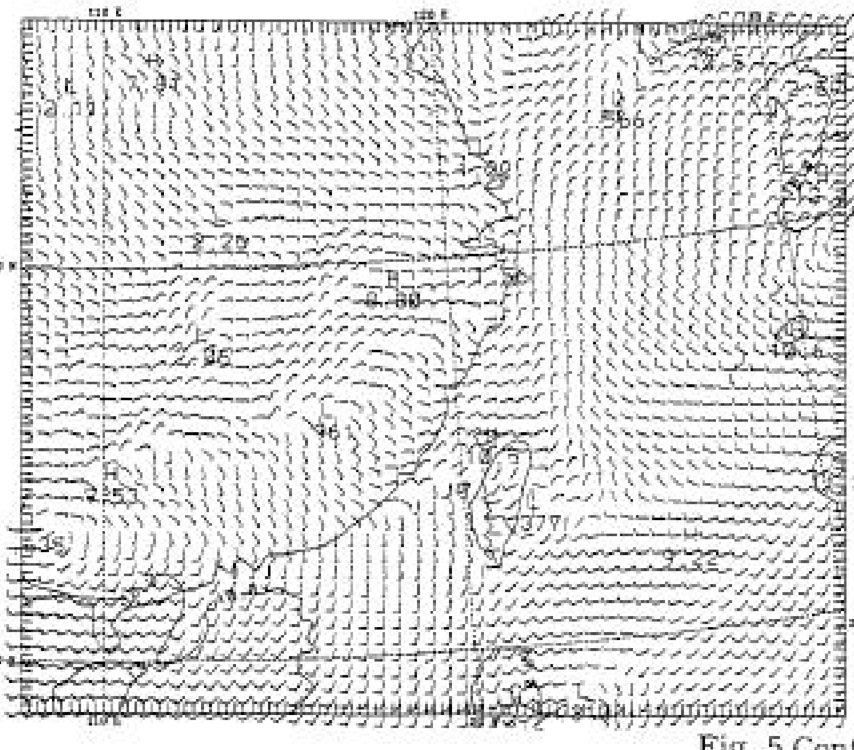

(d)

Fig. 5 Continued

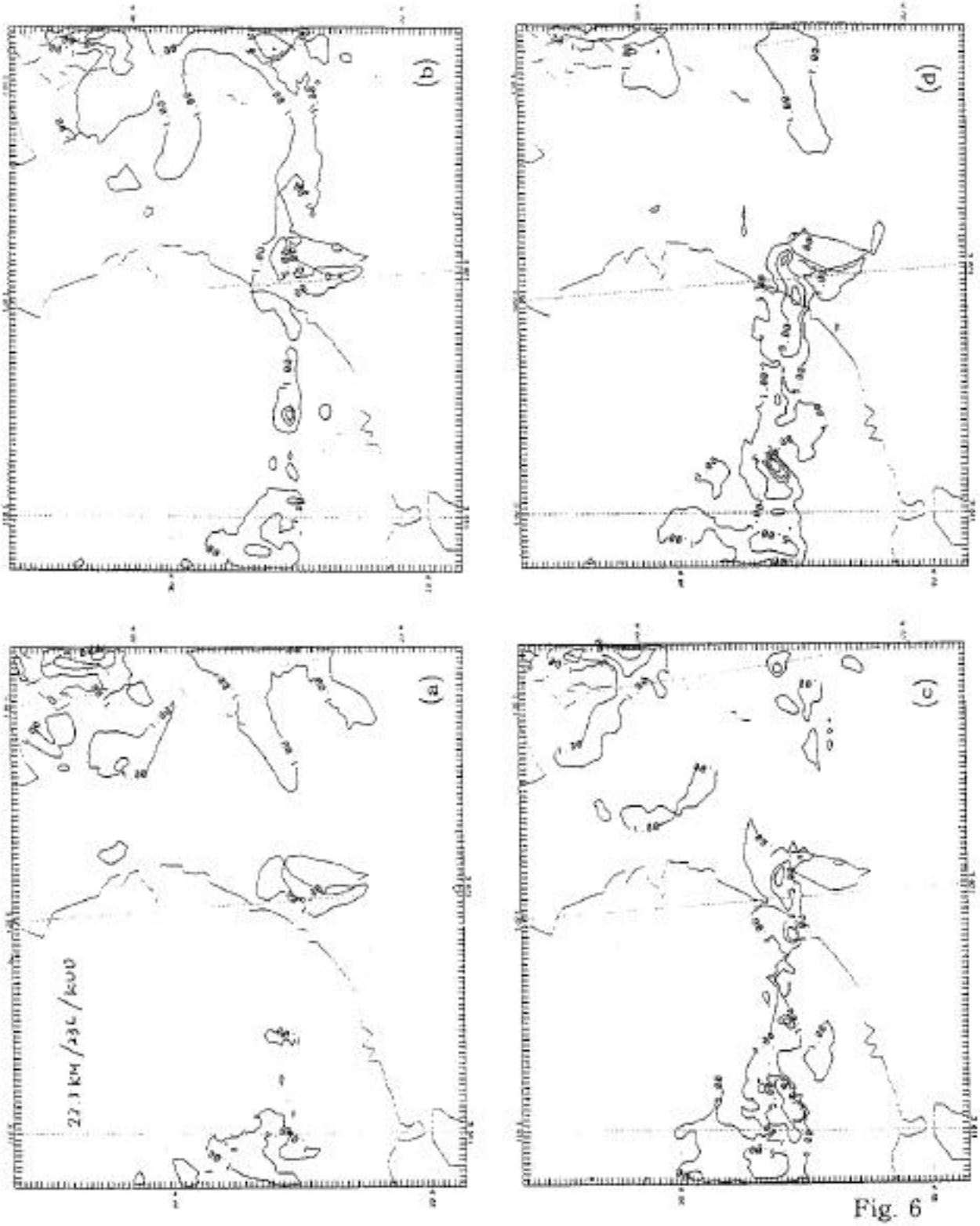

Fig. 6

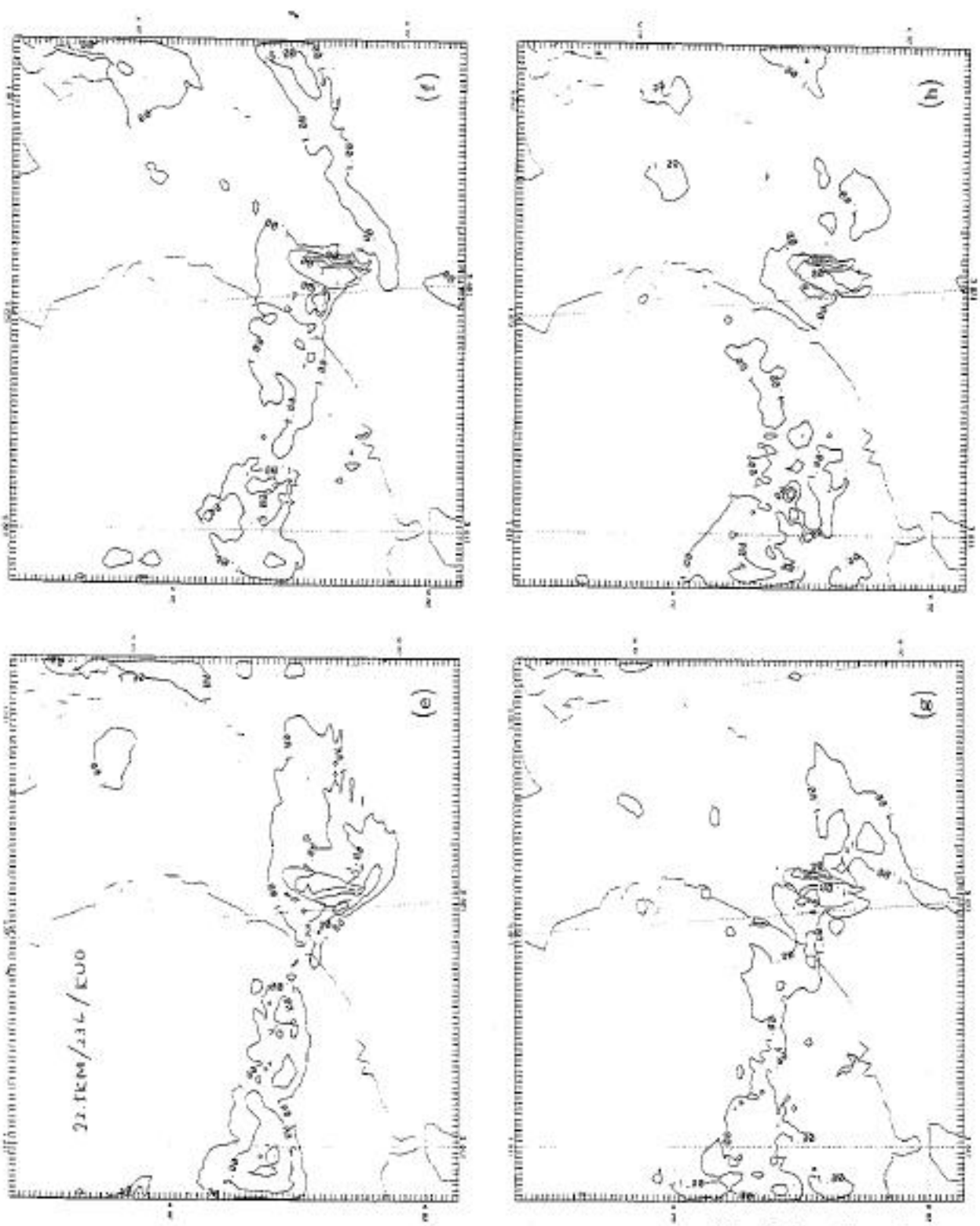

Fig. 6 Continued

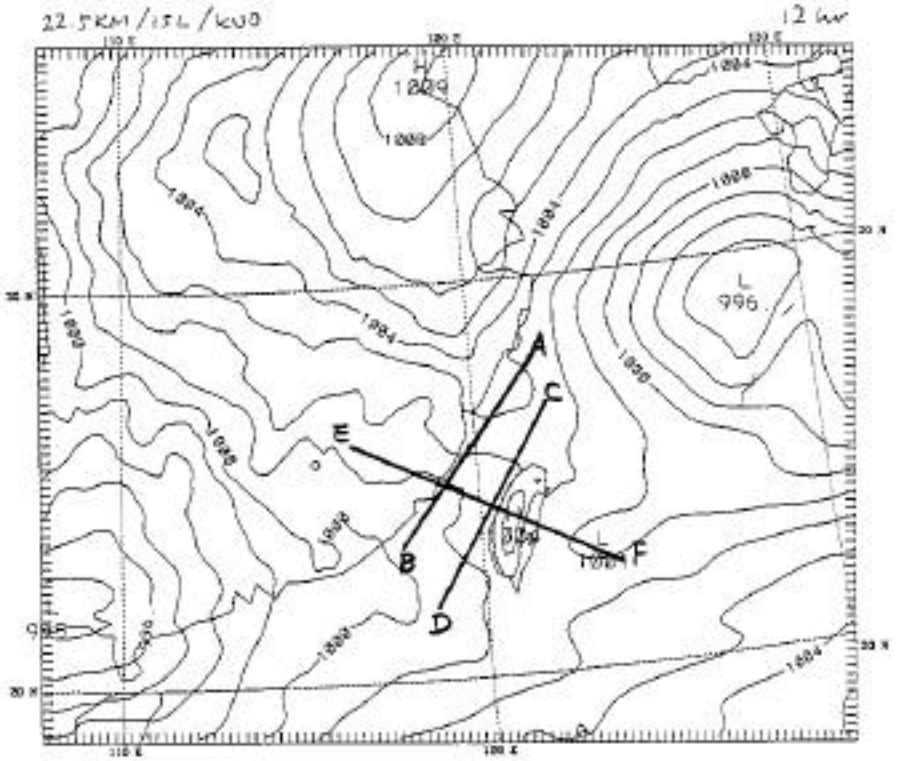

(a)

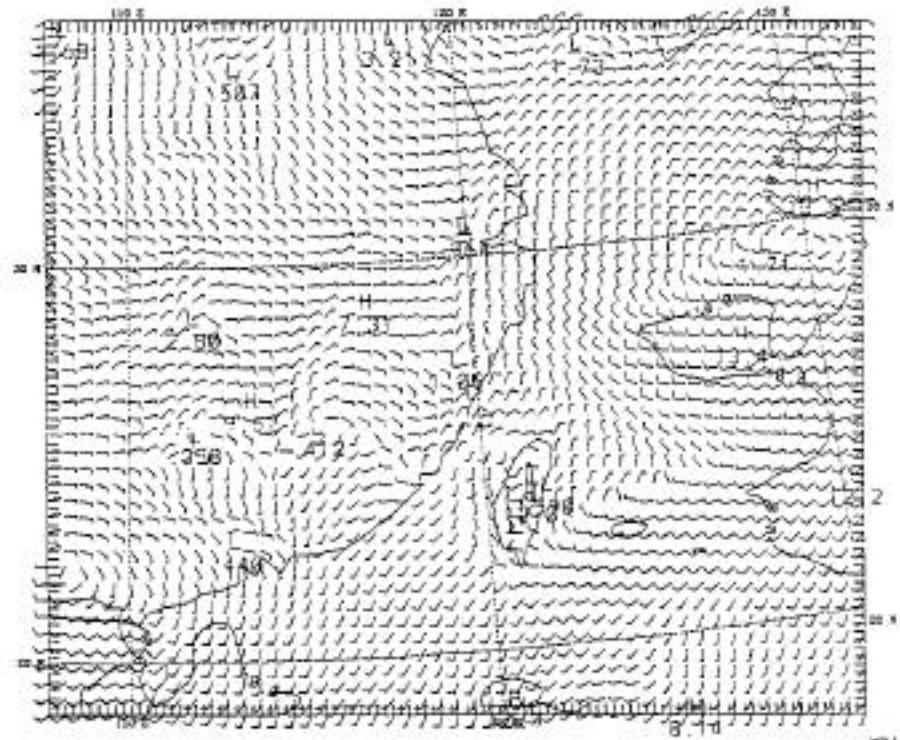

(b)

Fig. 7

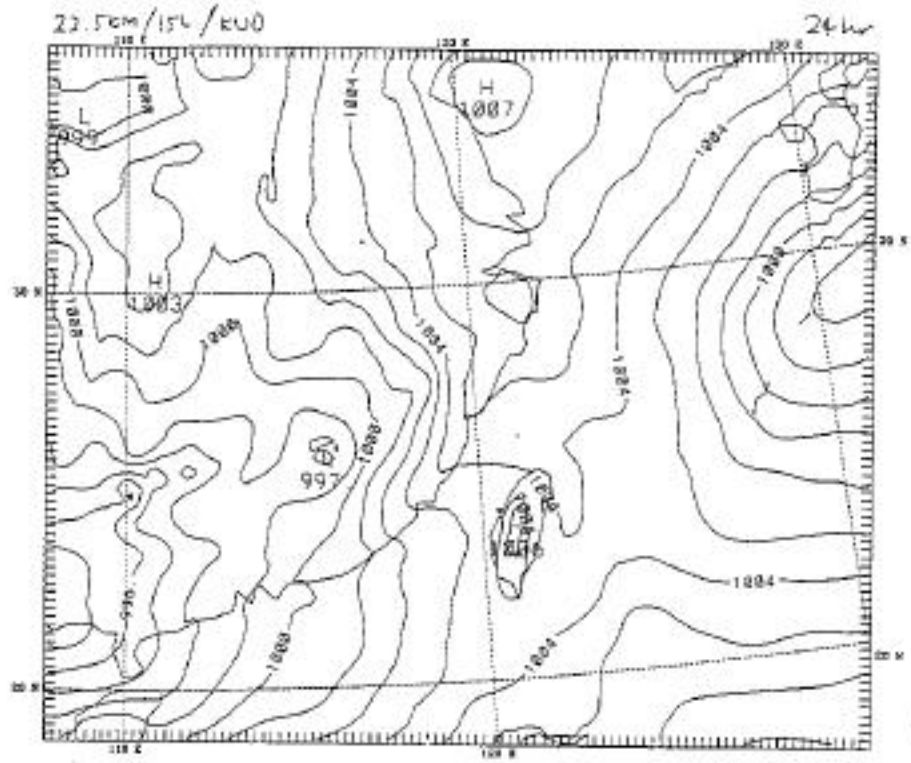

(c)

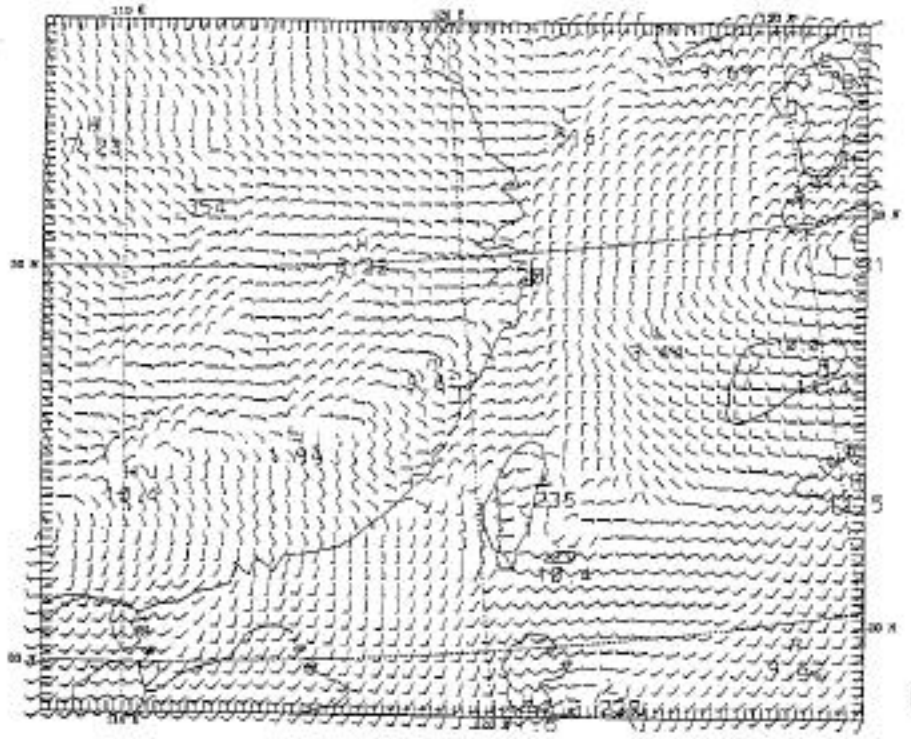

(d)

Fig. 7 Continued

Fig. 8

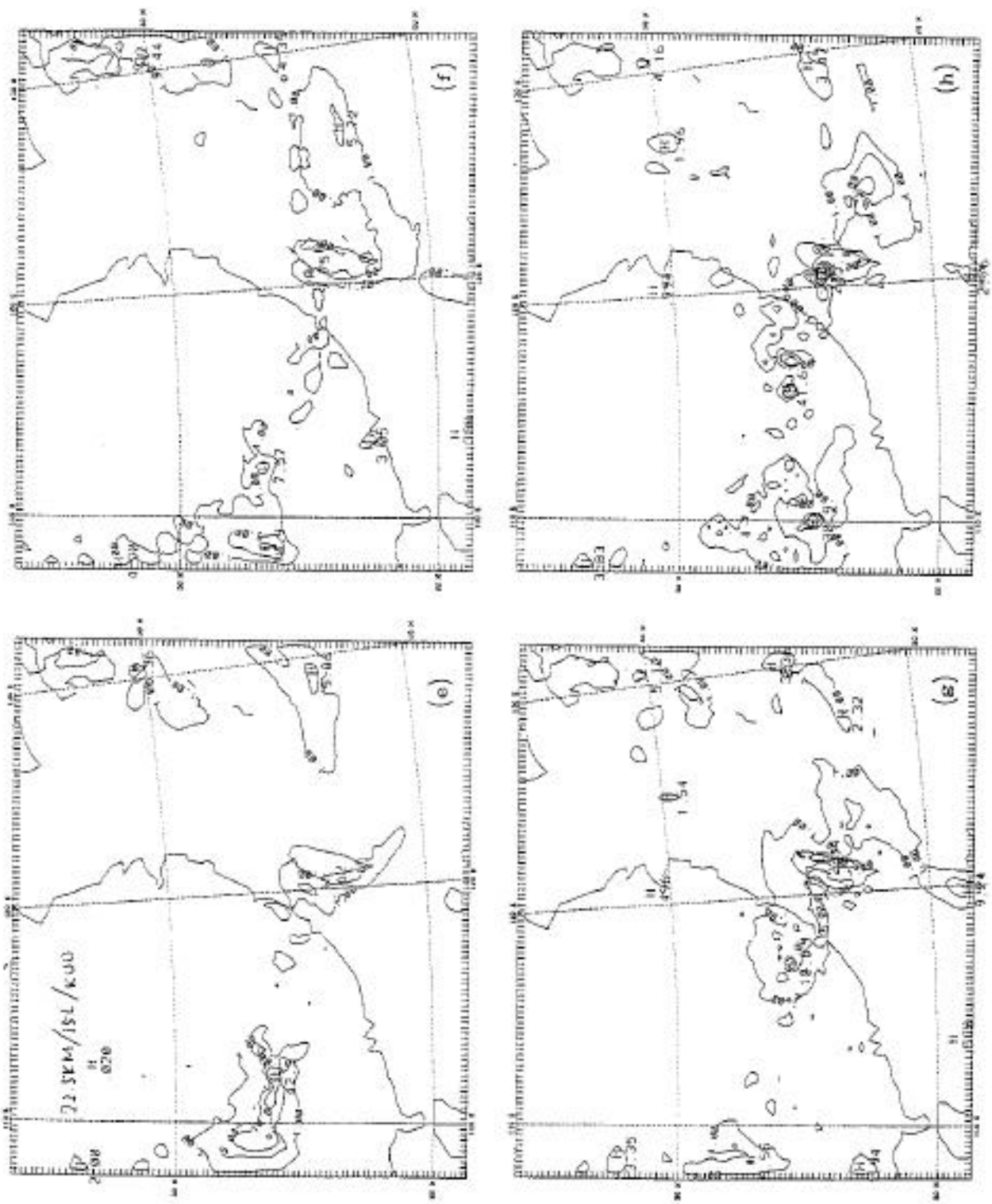

Fig. 8 Continued

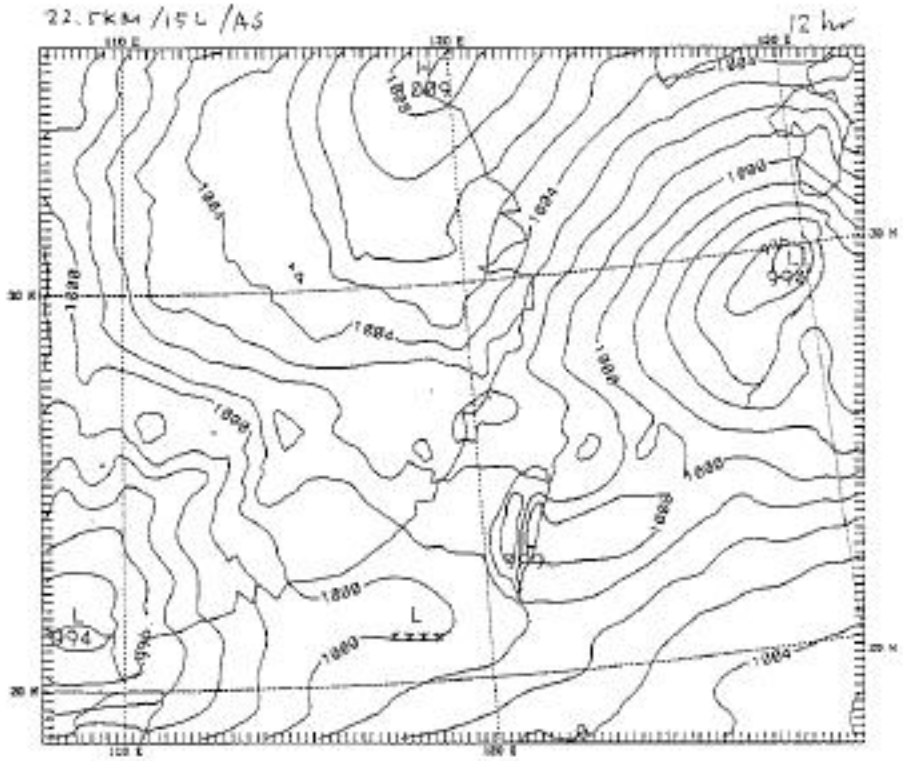

(a)

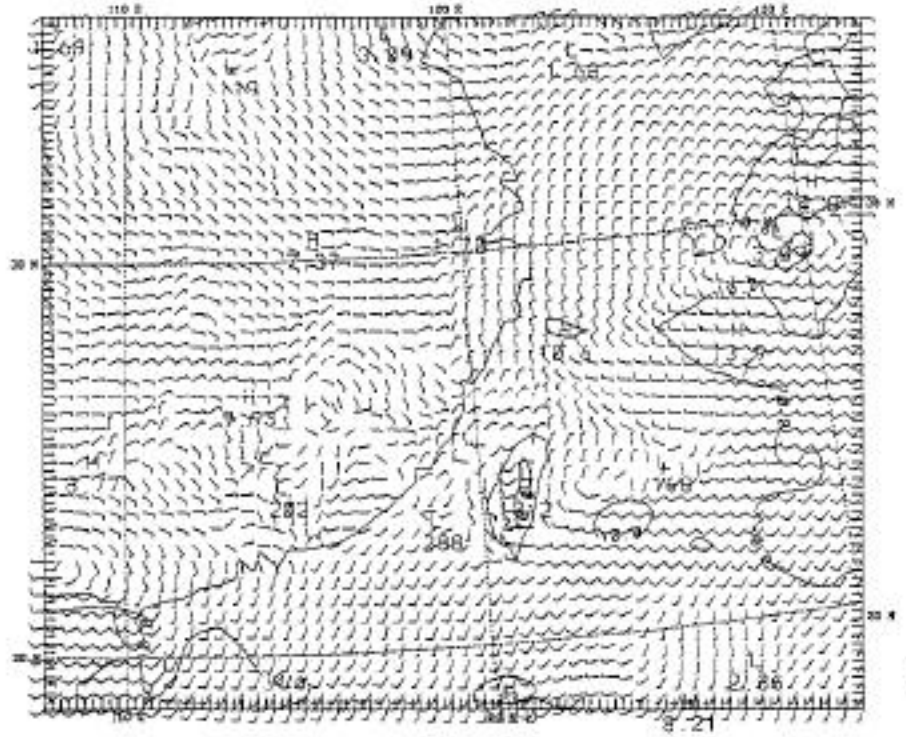

(b)

Fig. 9 Continued

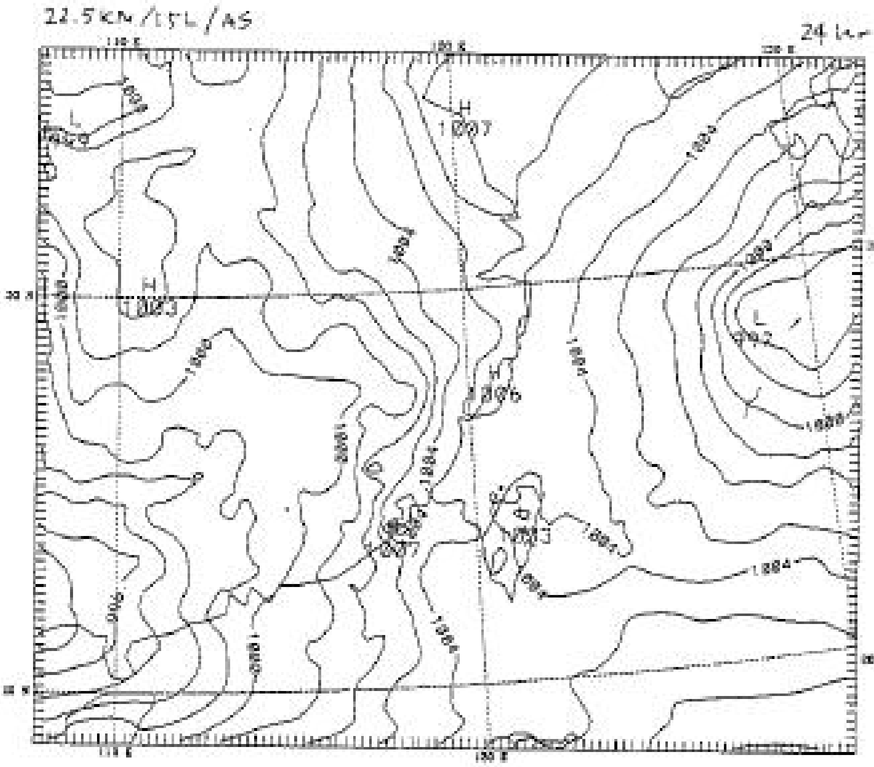

(c)

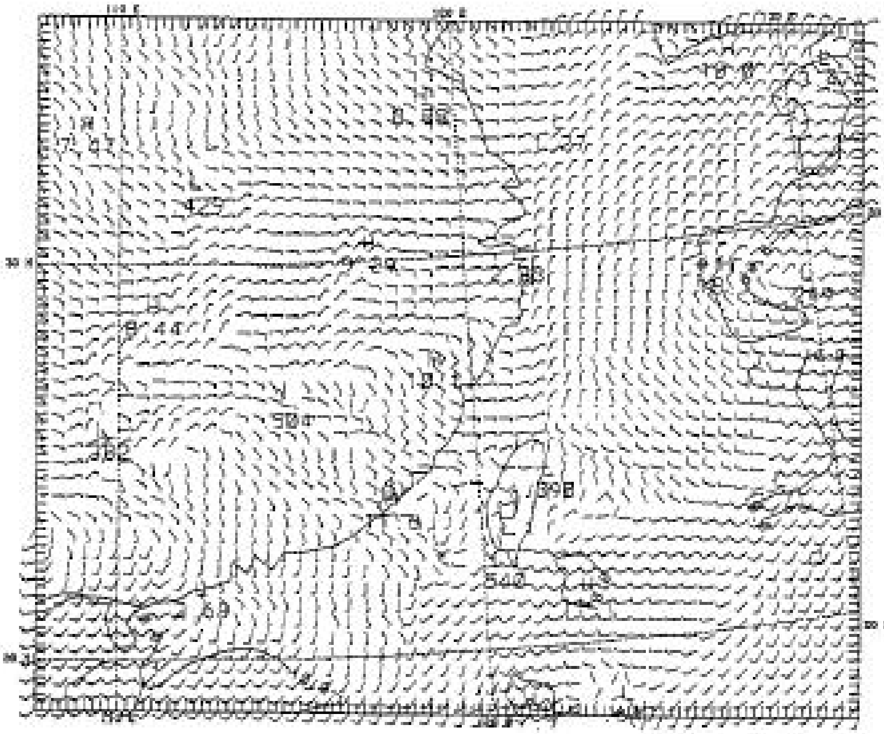

(d)

Fig. 9 Continued

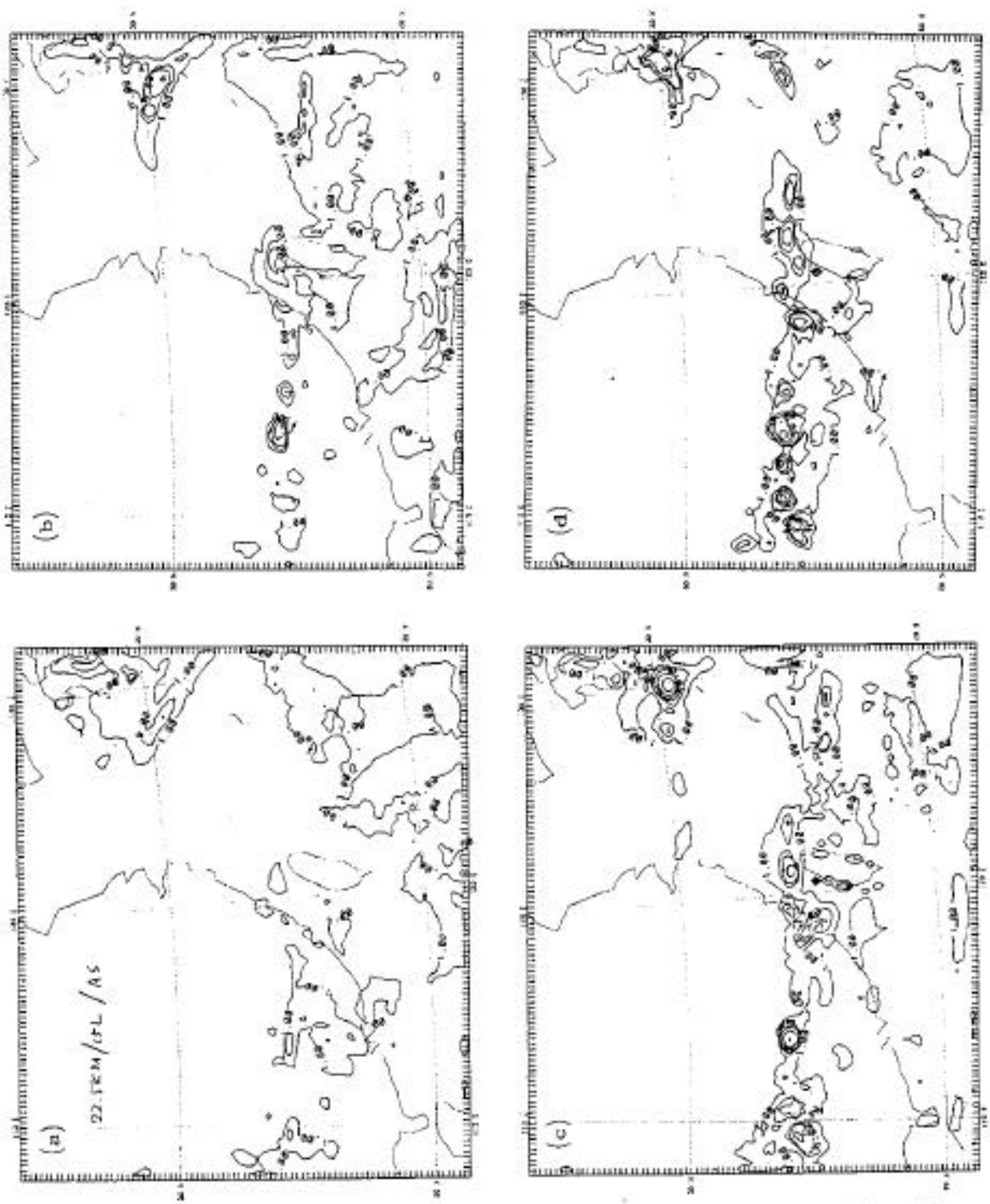

Fig. 10

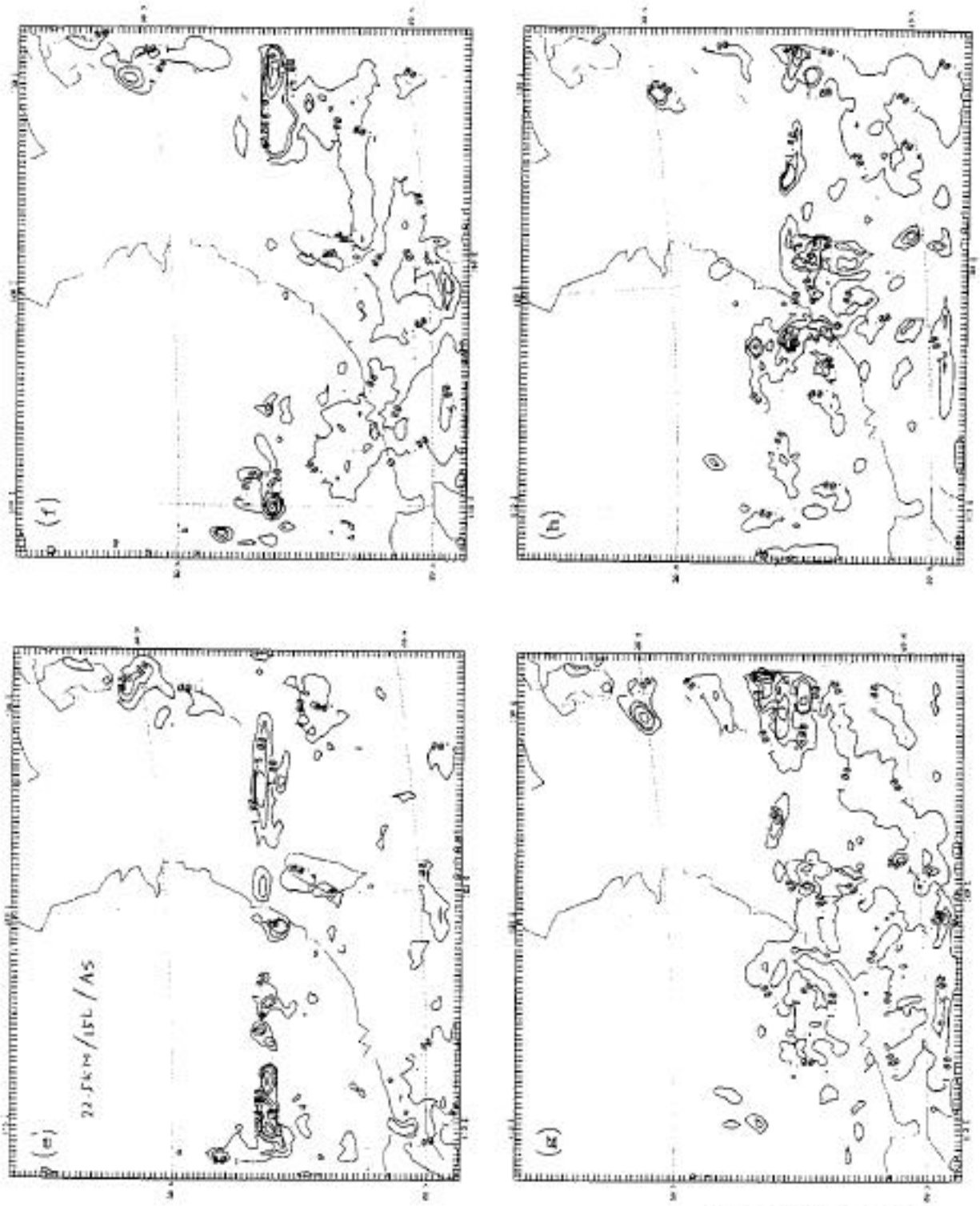

Fig. 10 Continued

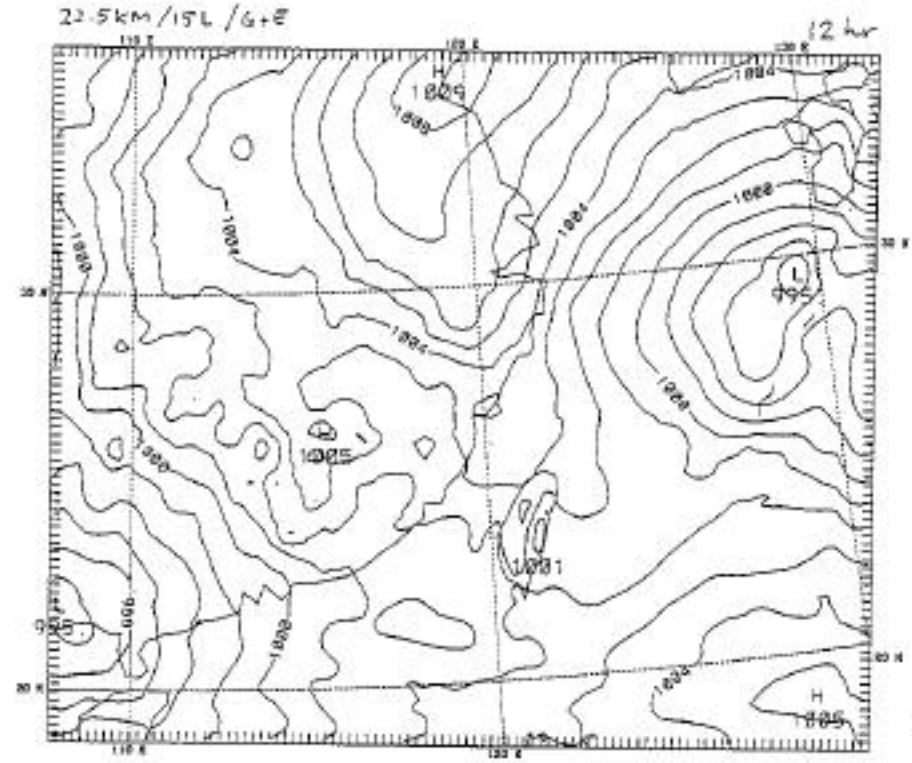

Fig. 11

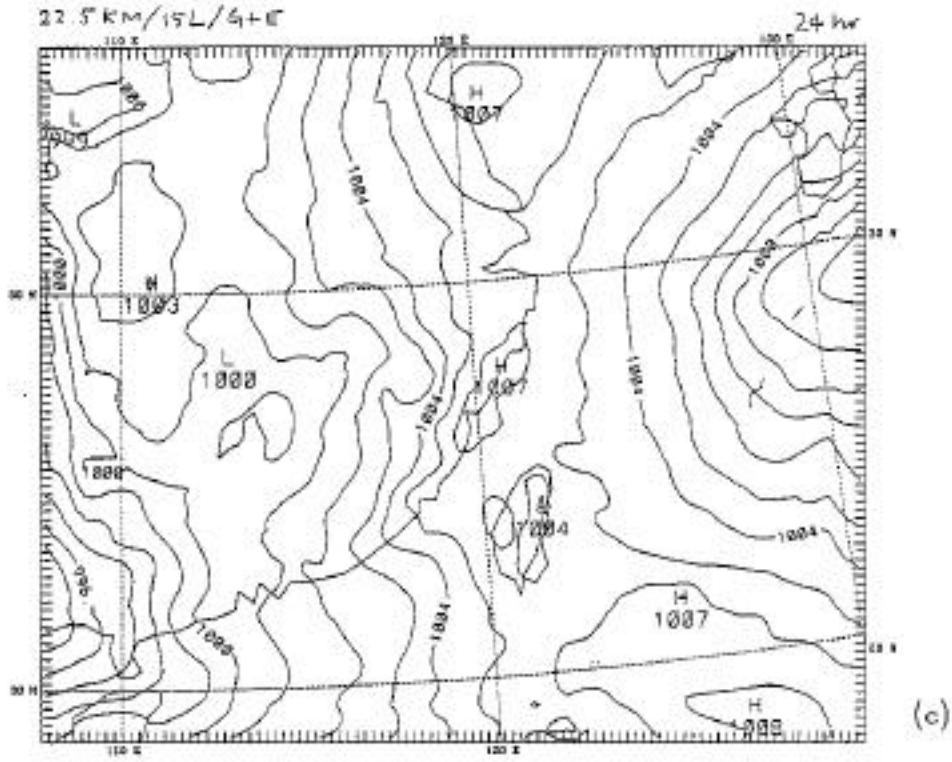

(c)

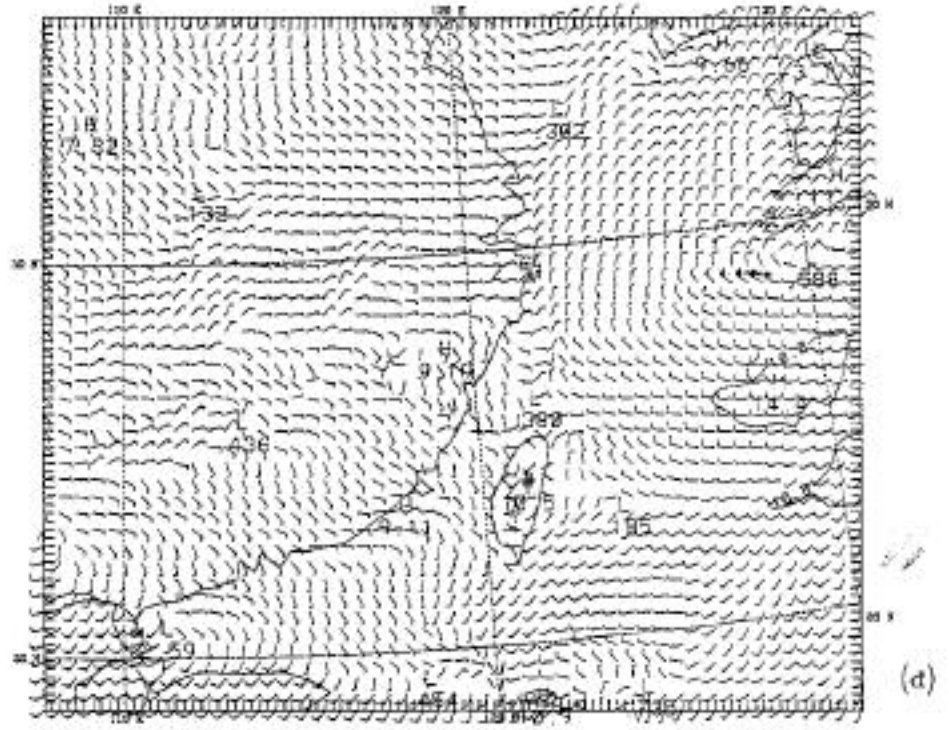

(d)

Fig. 11 Continued

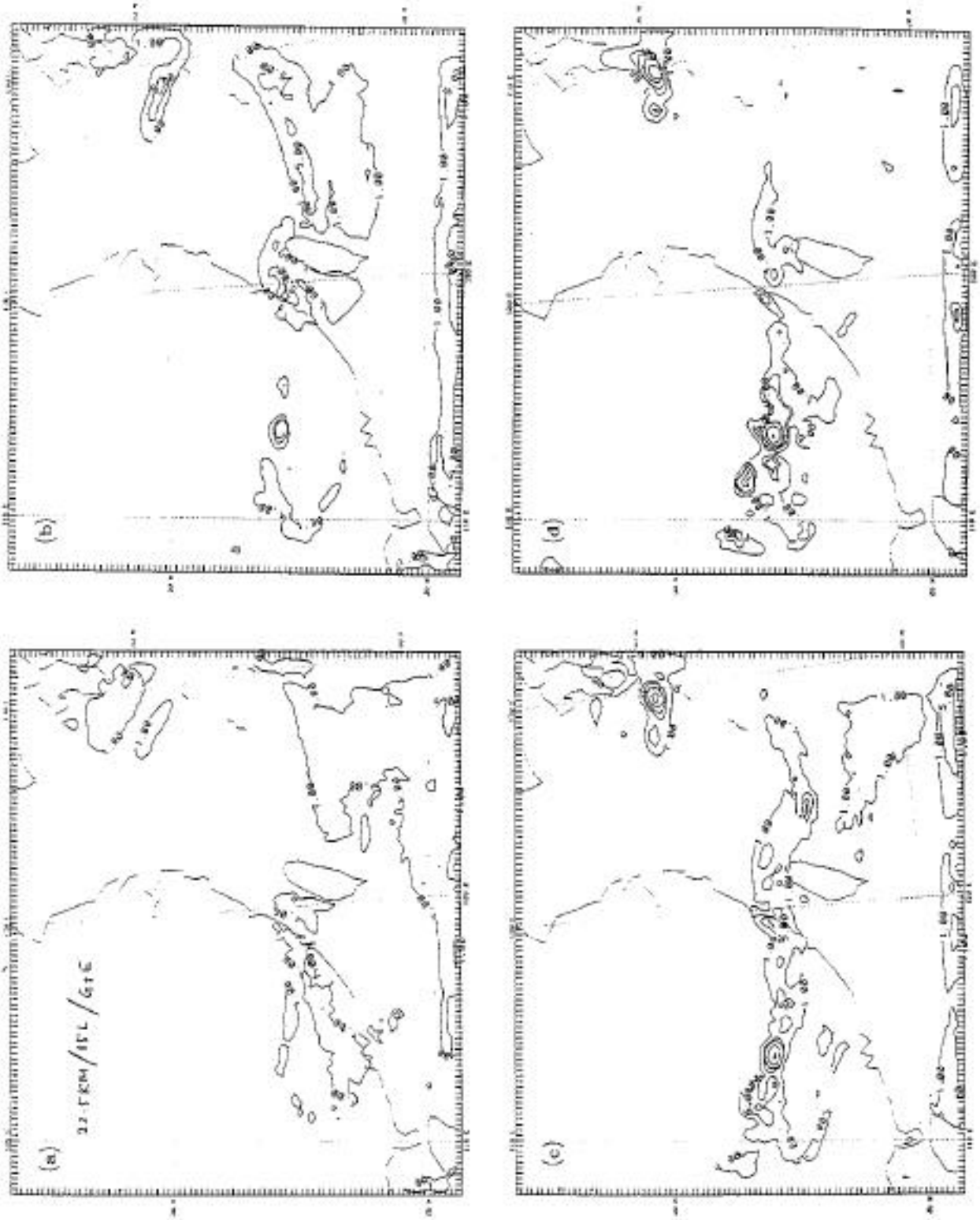

Fig. 12

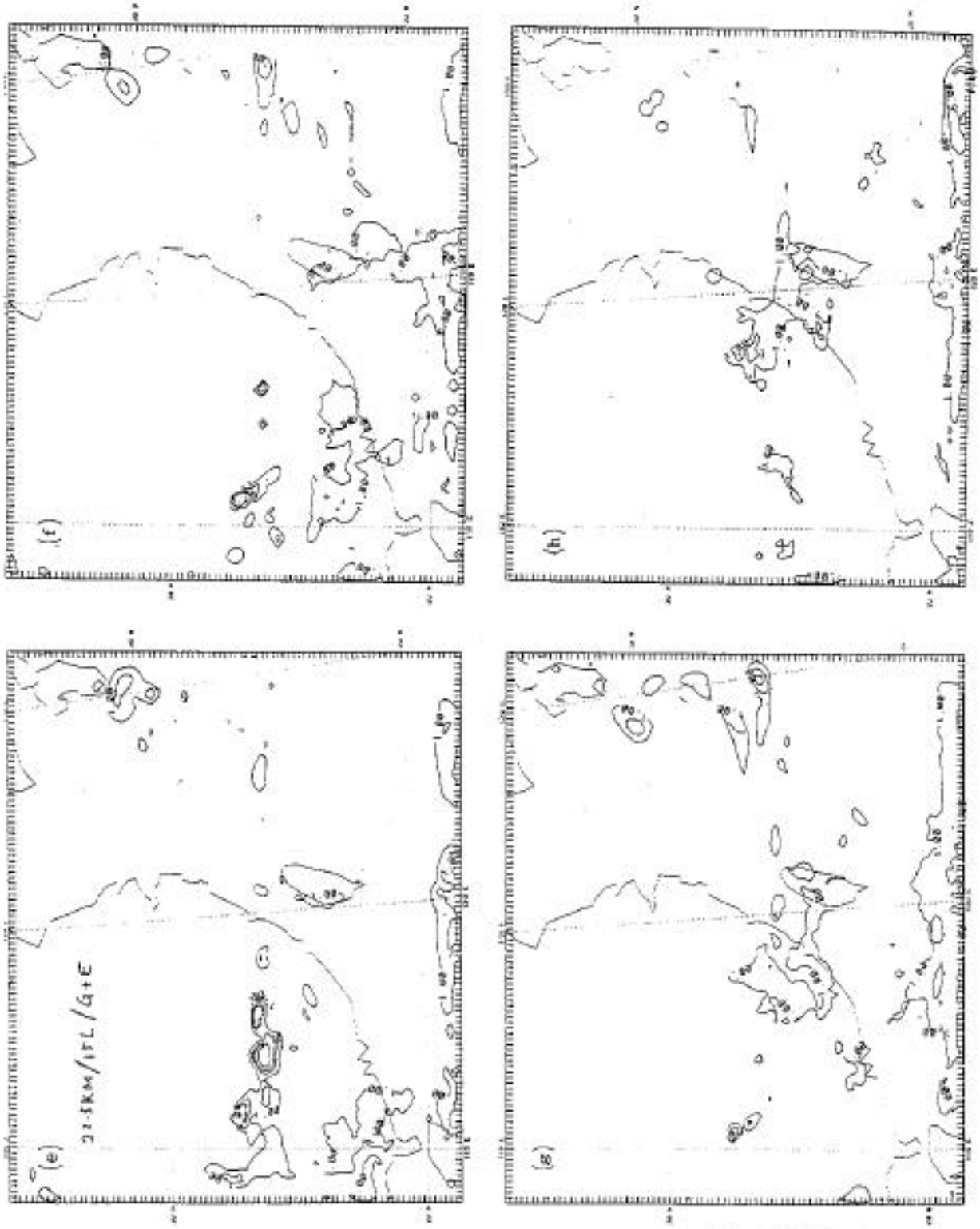

Fig. 12 Continued

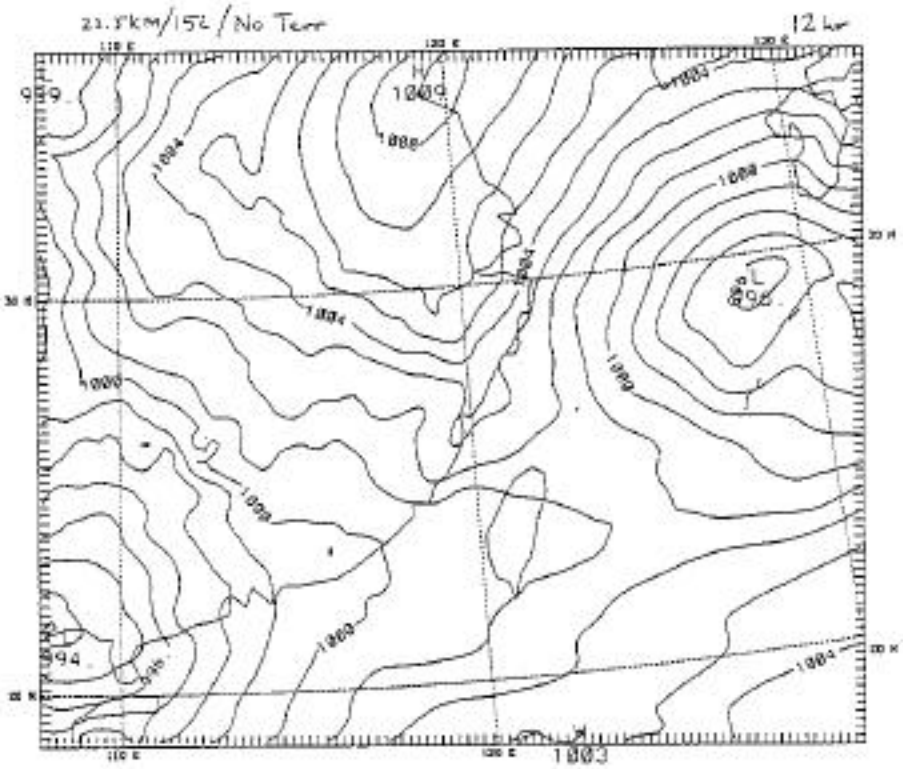

(a)

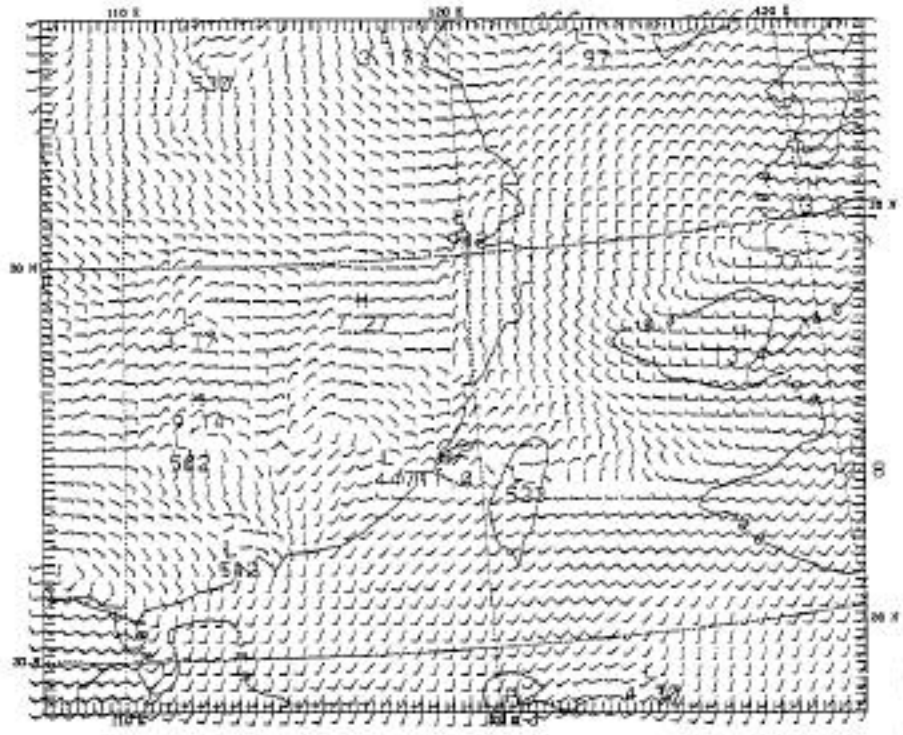

(b)

Fig. 13

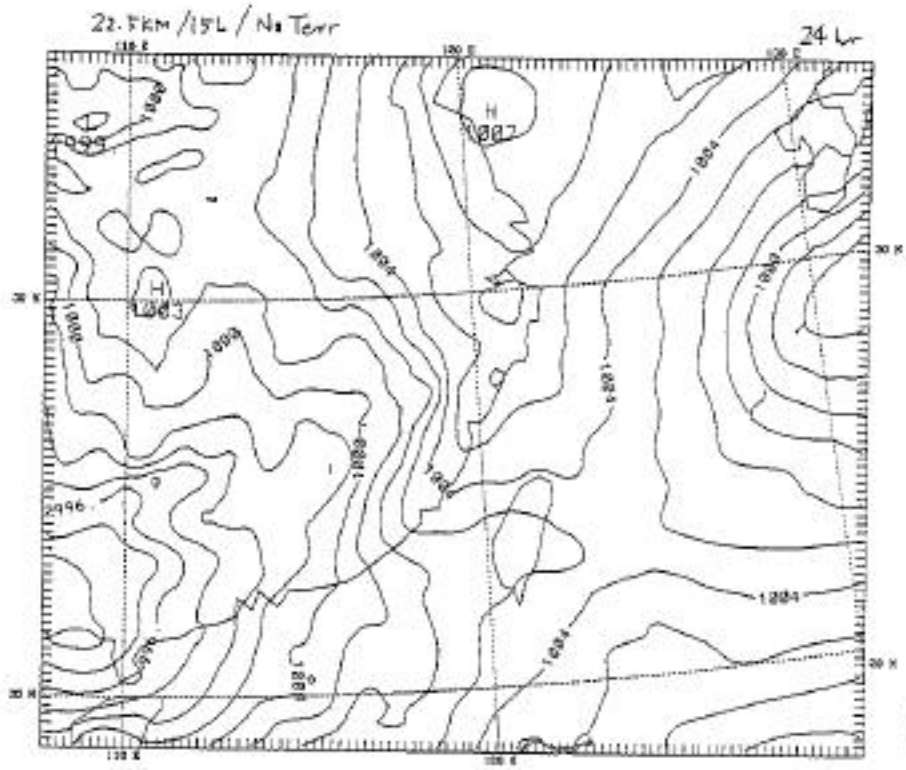

(c)

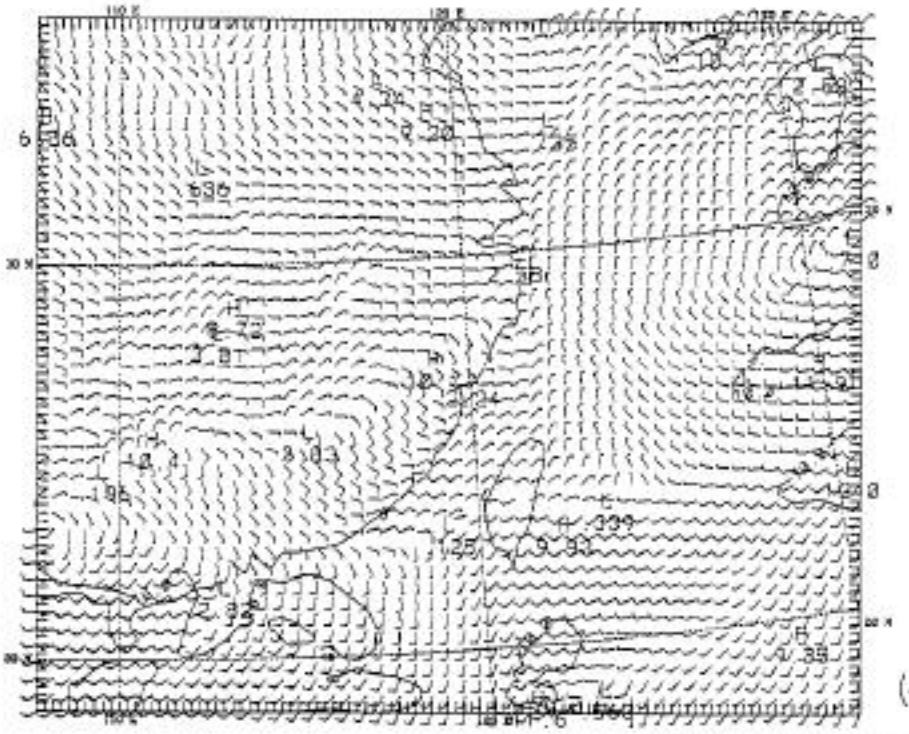

(d)

Fig. 13 Continued

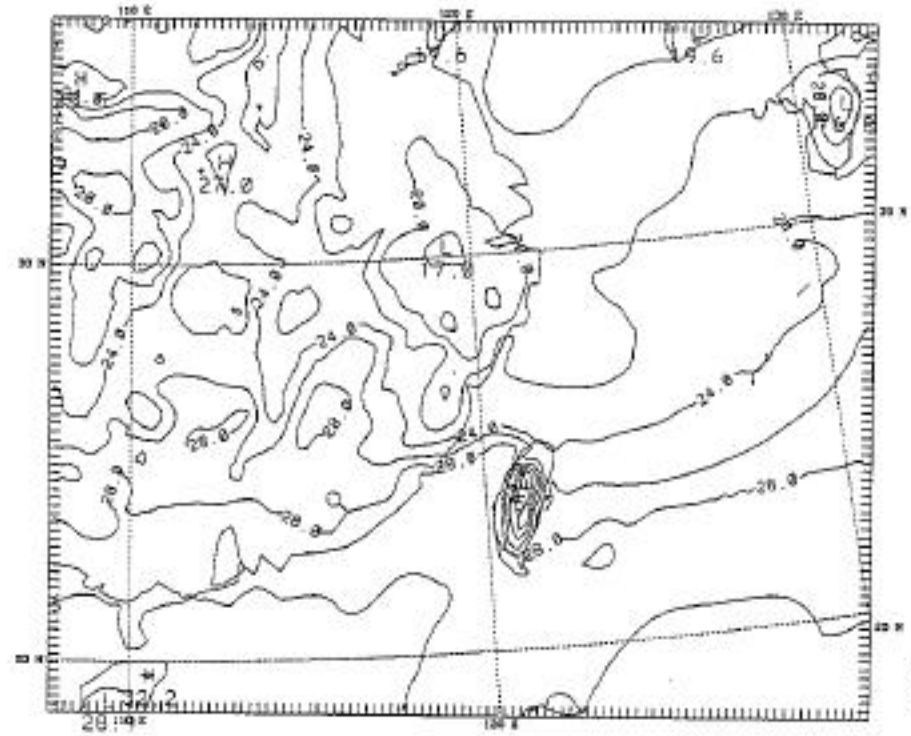

(a)

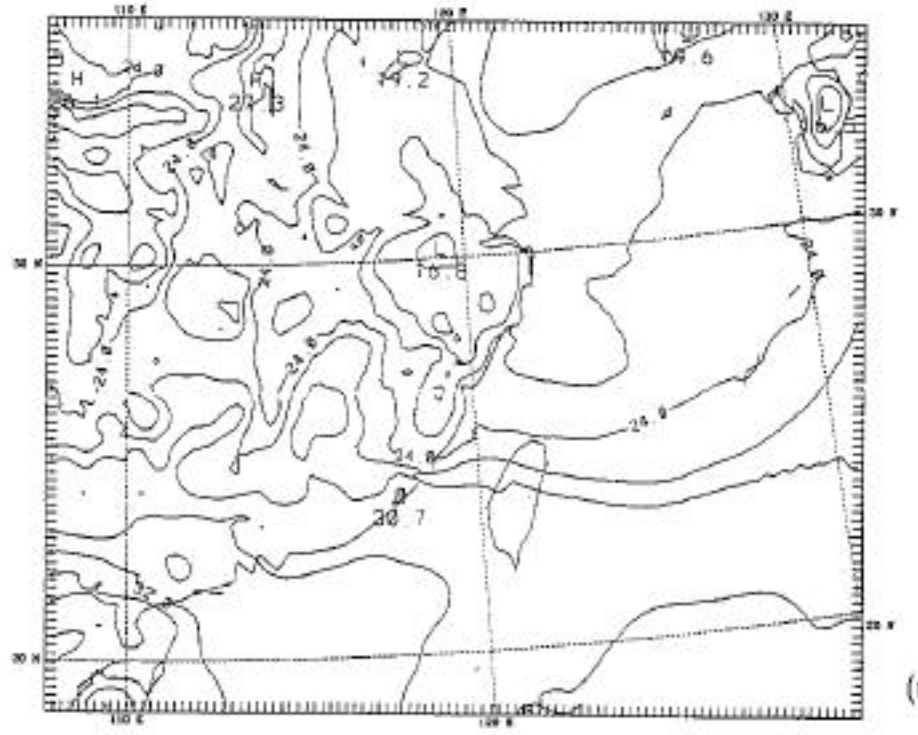

(b)

Fig. 14

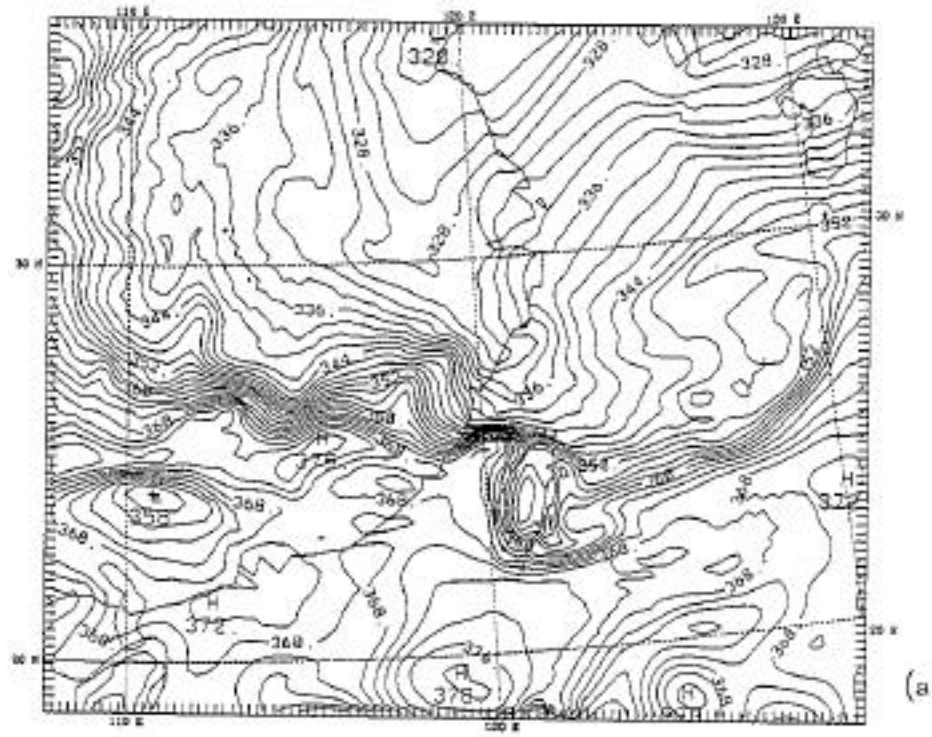

Fig. 15

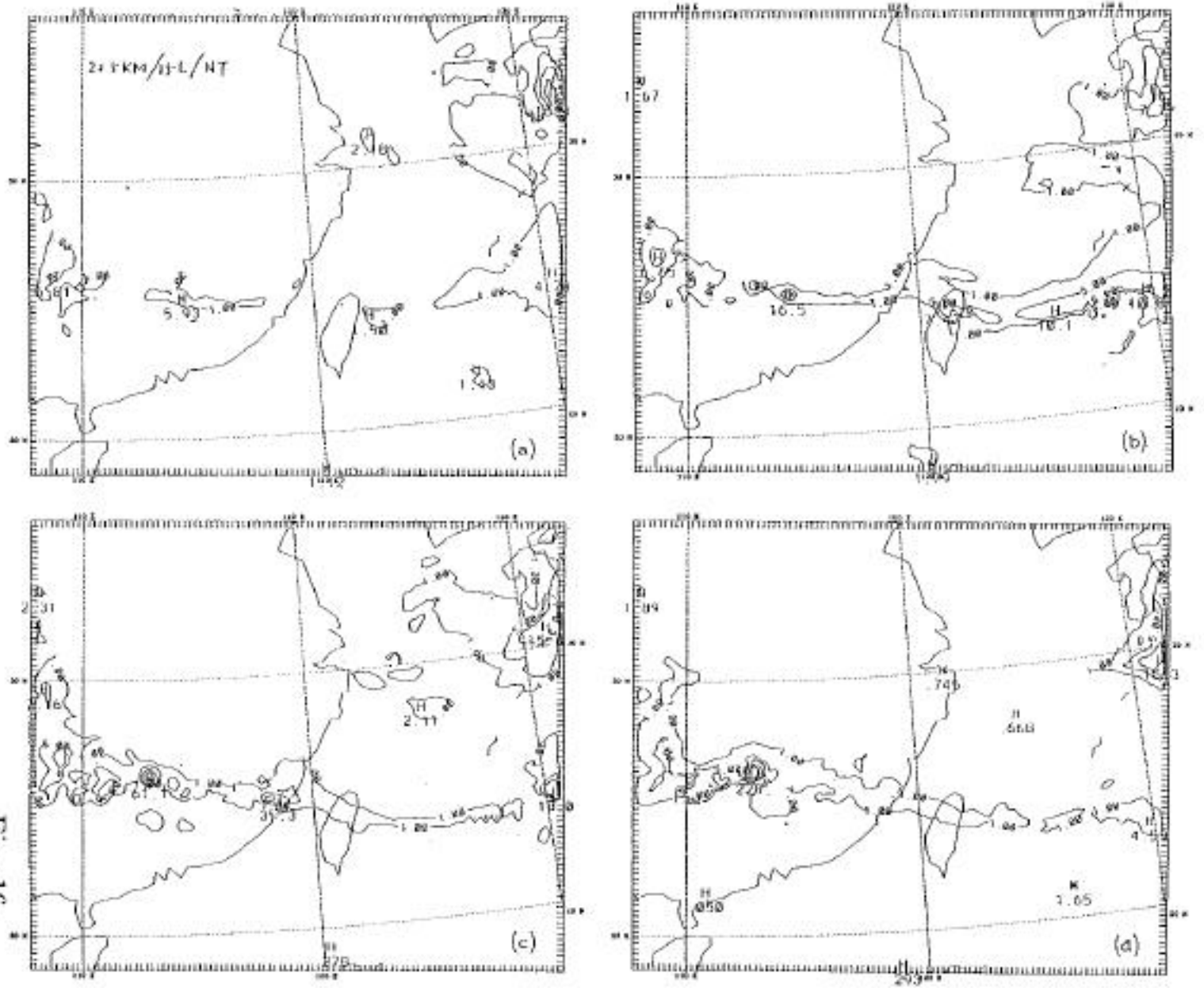

Fig. 16

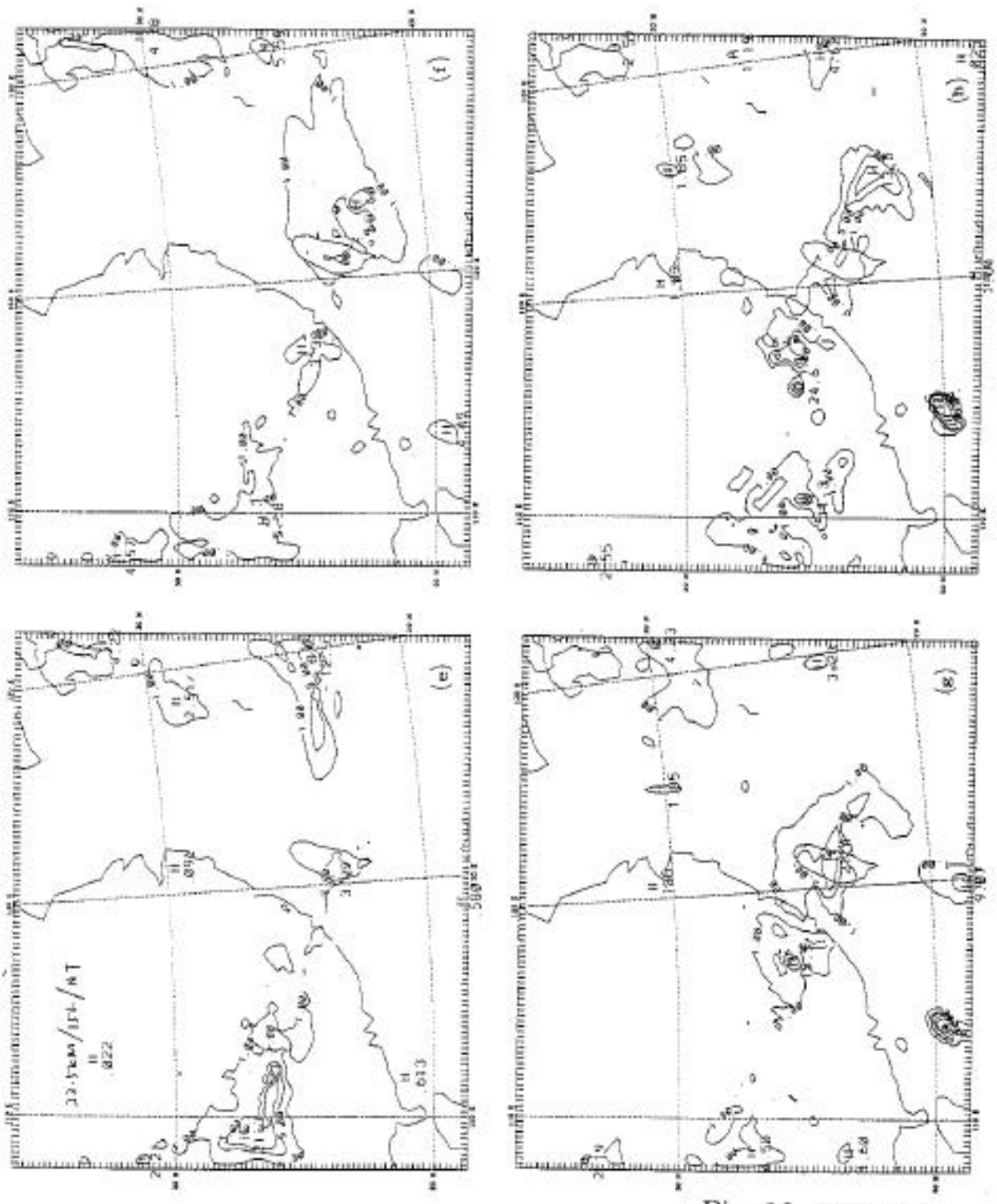

Fig. 16 Continued

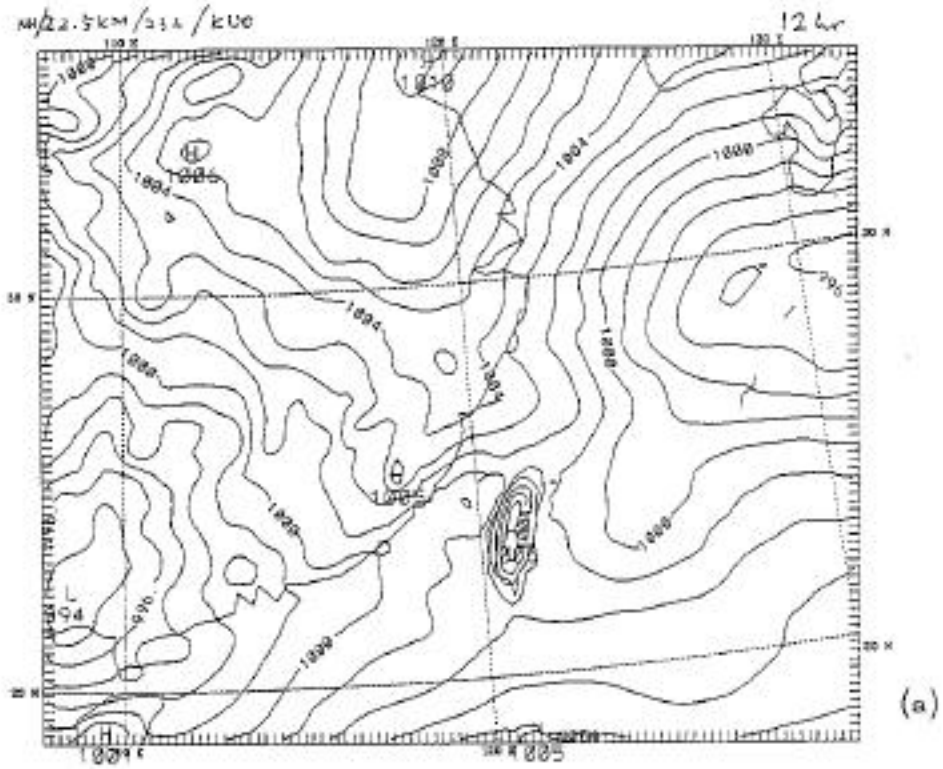

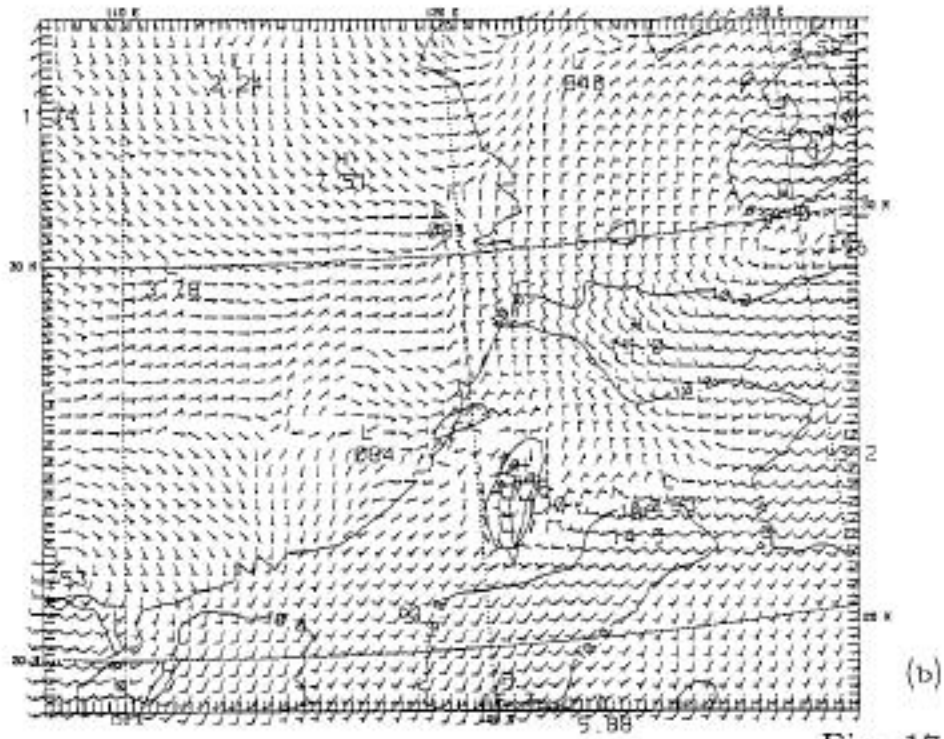

Fig. 17

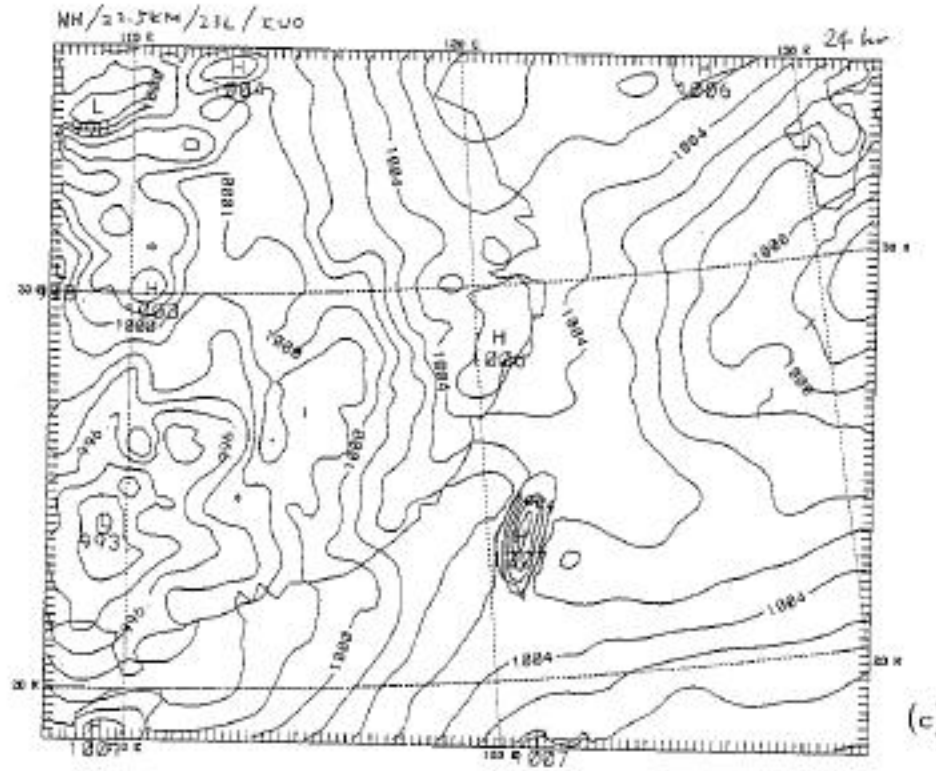

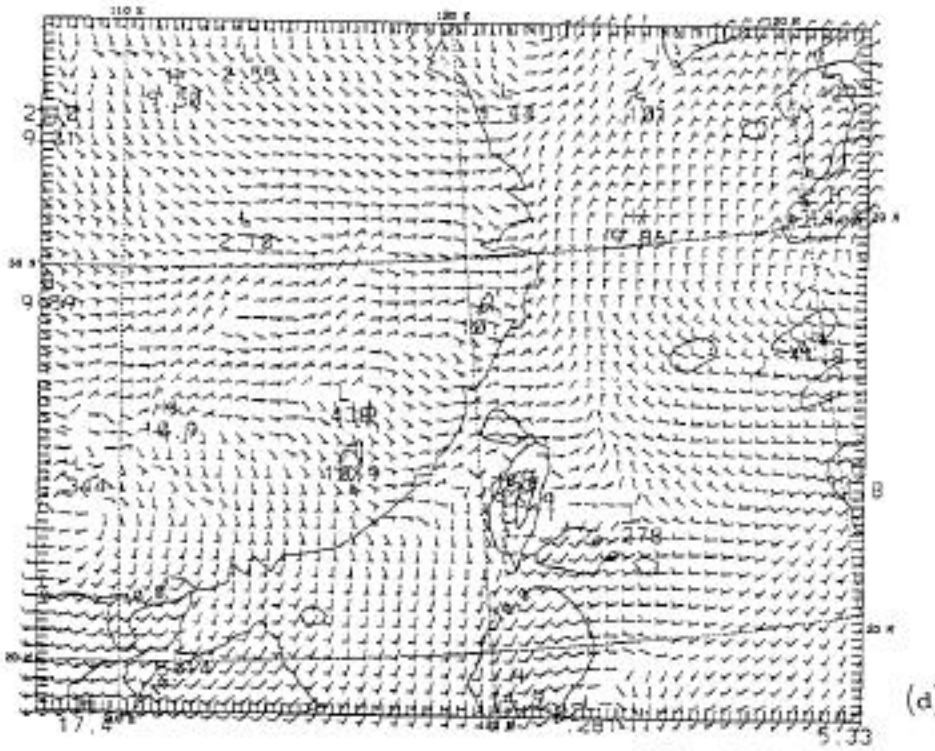

Fig. 17 Continued

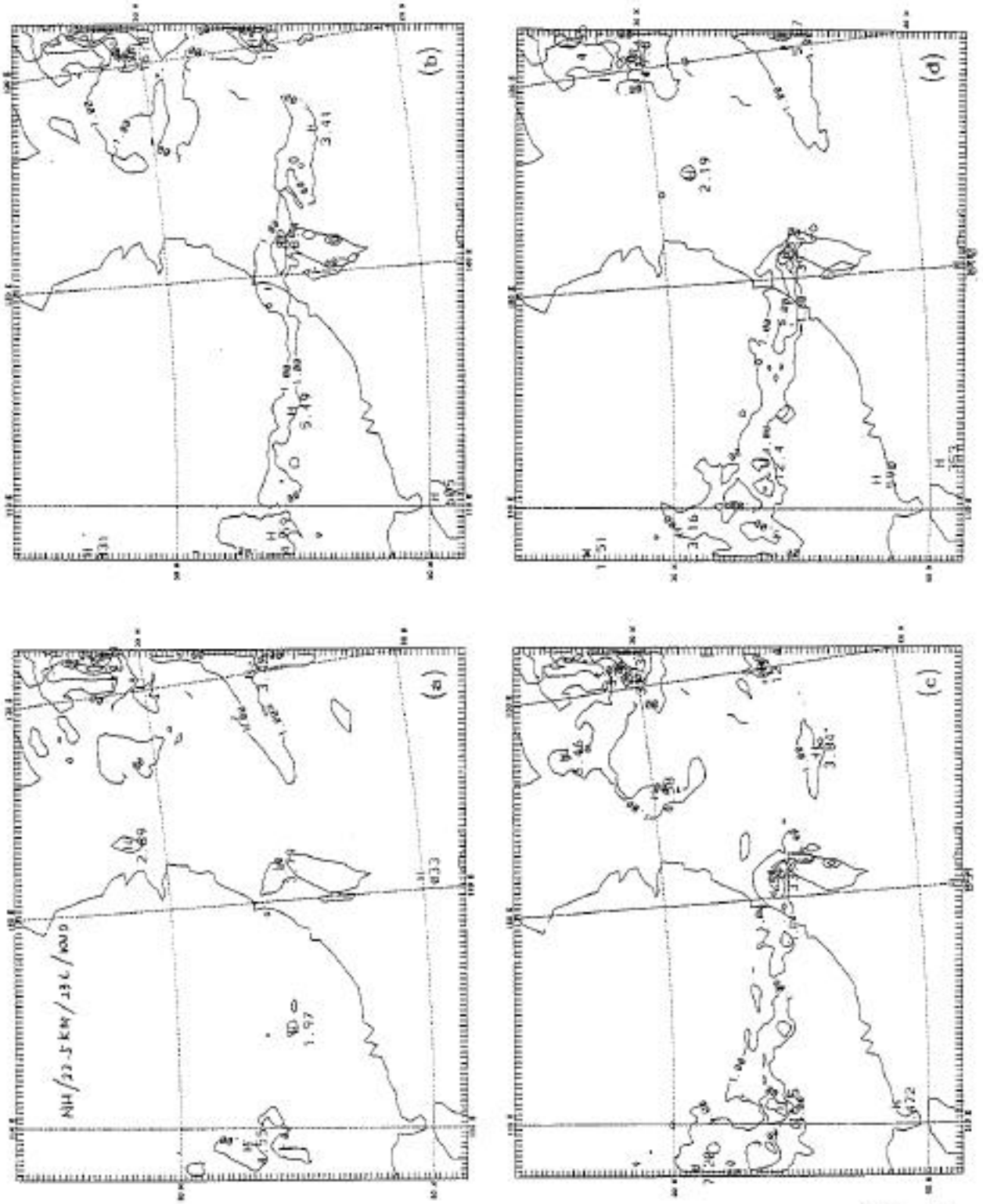

Fig. 18

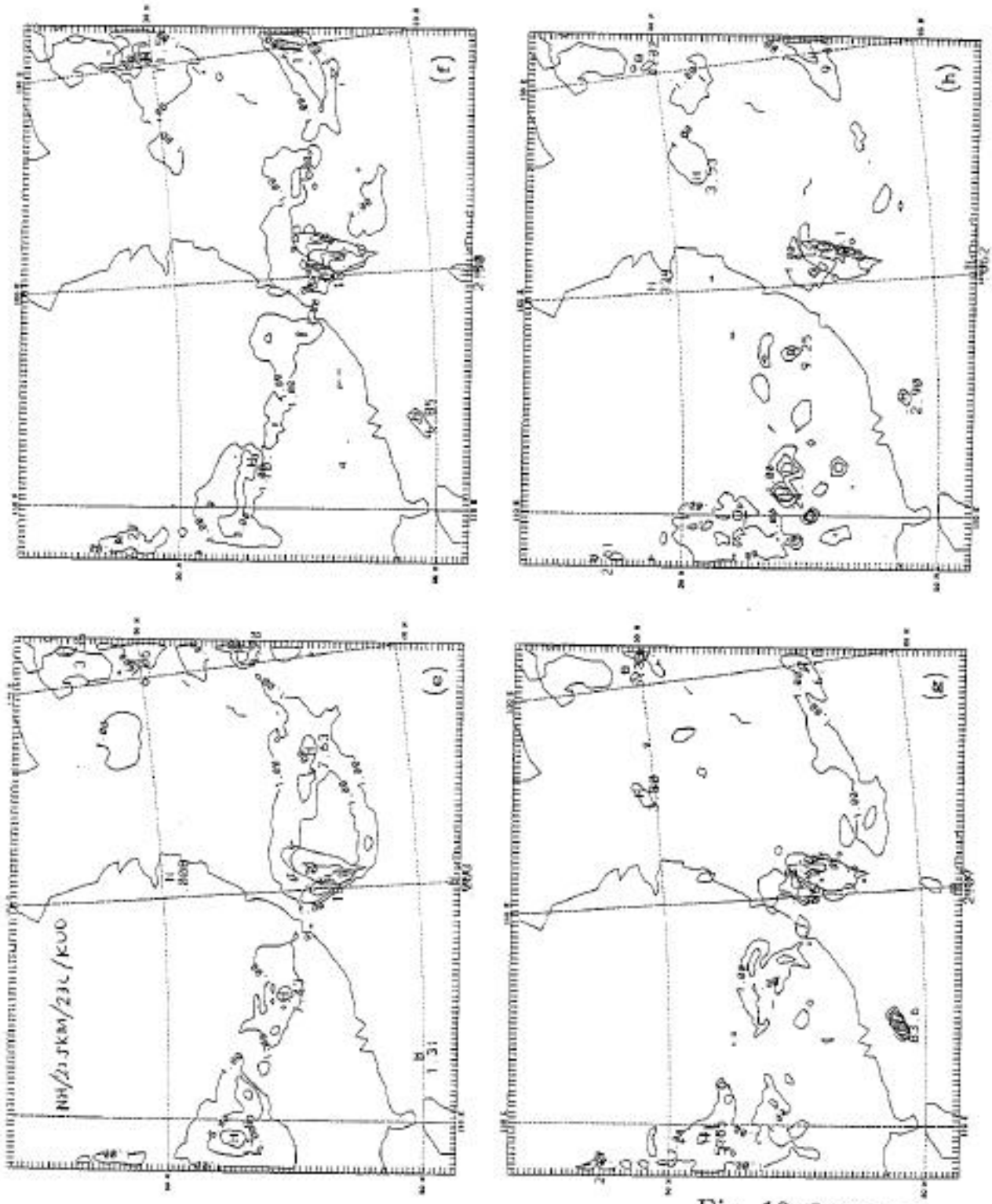

Fig. 18 Continued

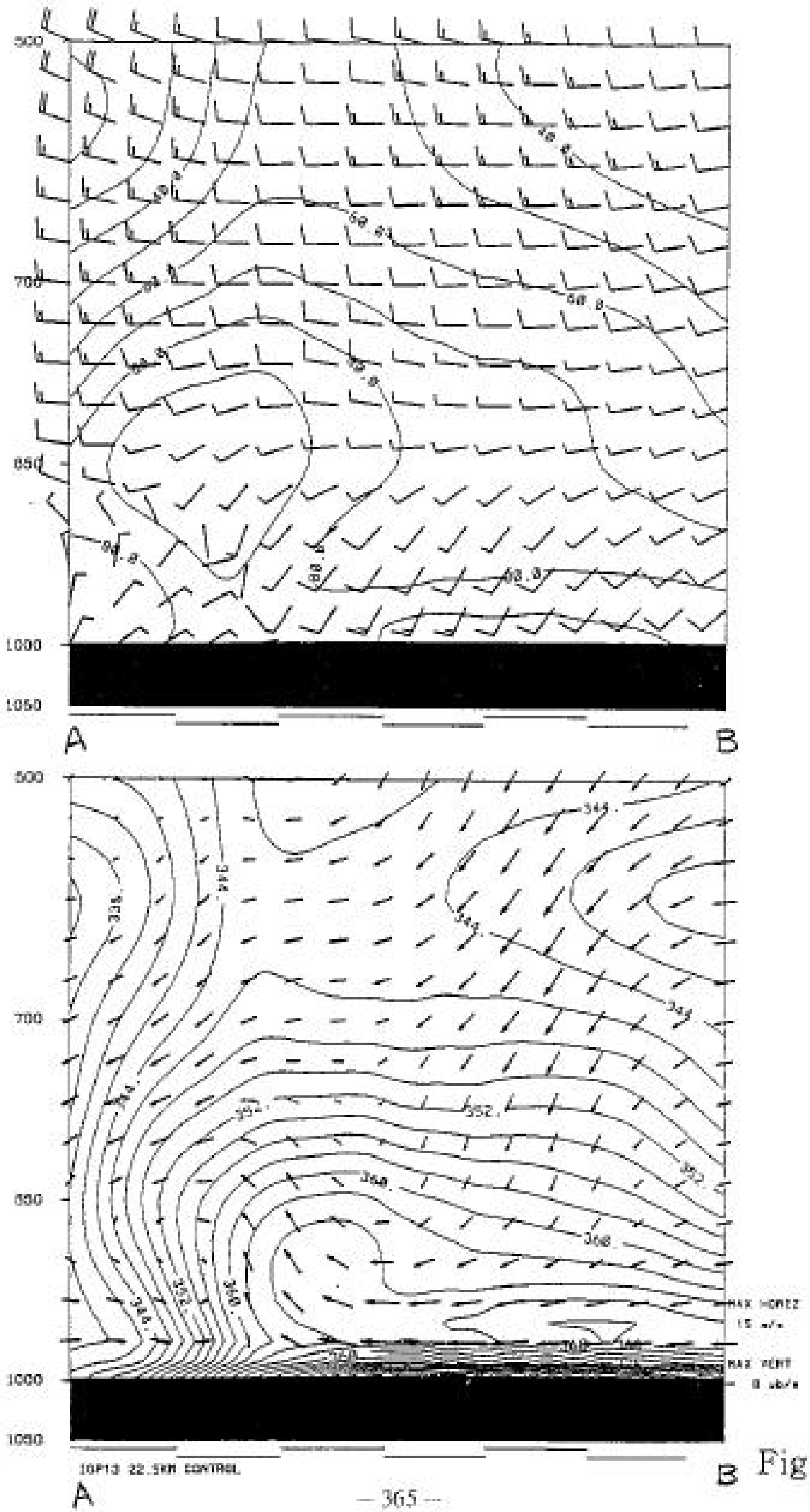
500
700
850
1000
1050
A
B
IOP13 22.5KM CONTROL
MAX HORIZ
15 m/s
MAX VERT
8 ub/s

(a)

Fig. 19

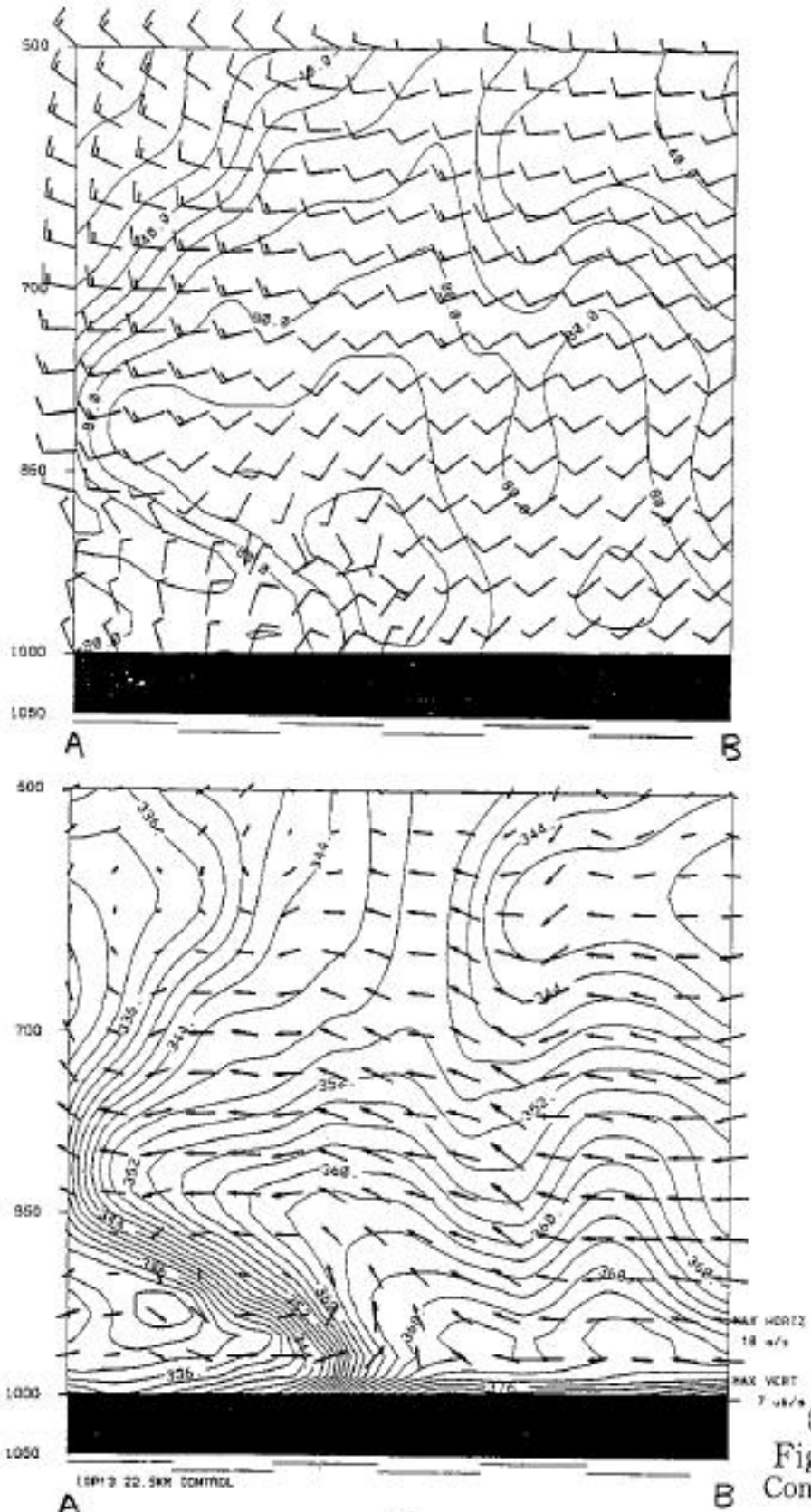

(b)

Fig. 19
Continued

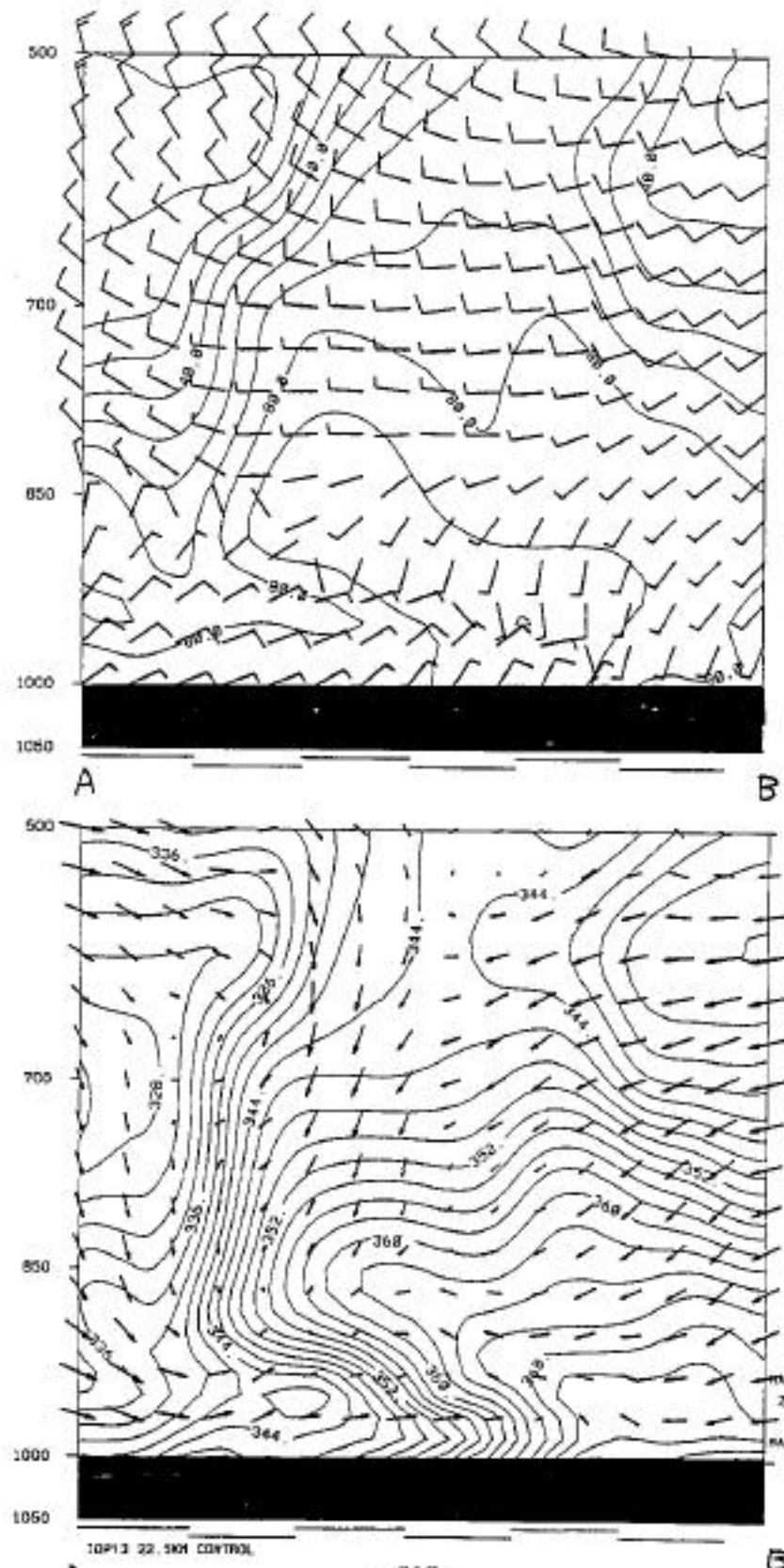

(c)

Fig. 19
Continued

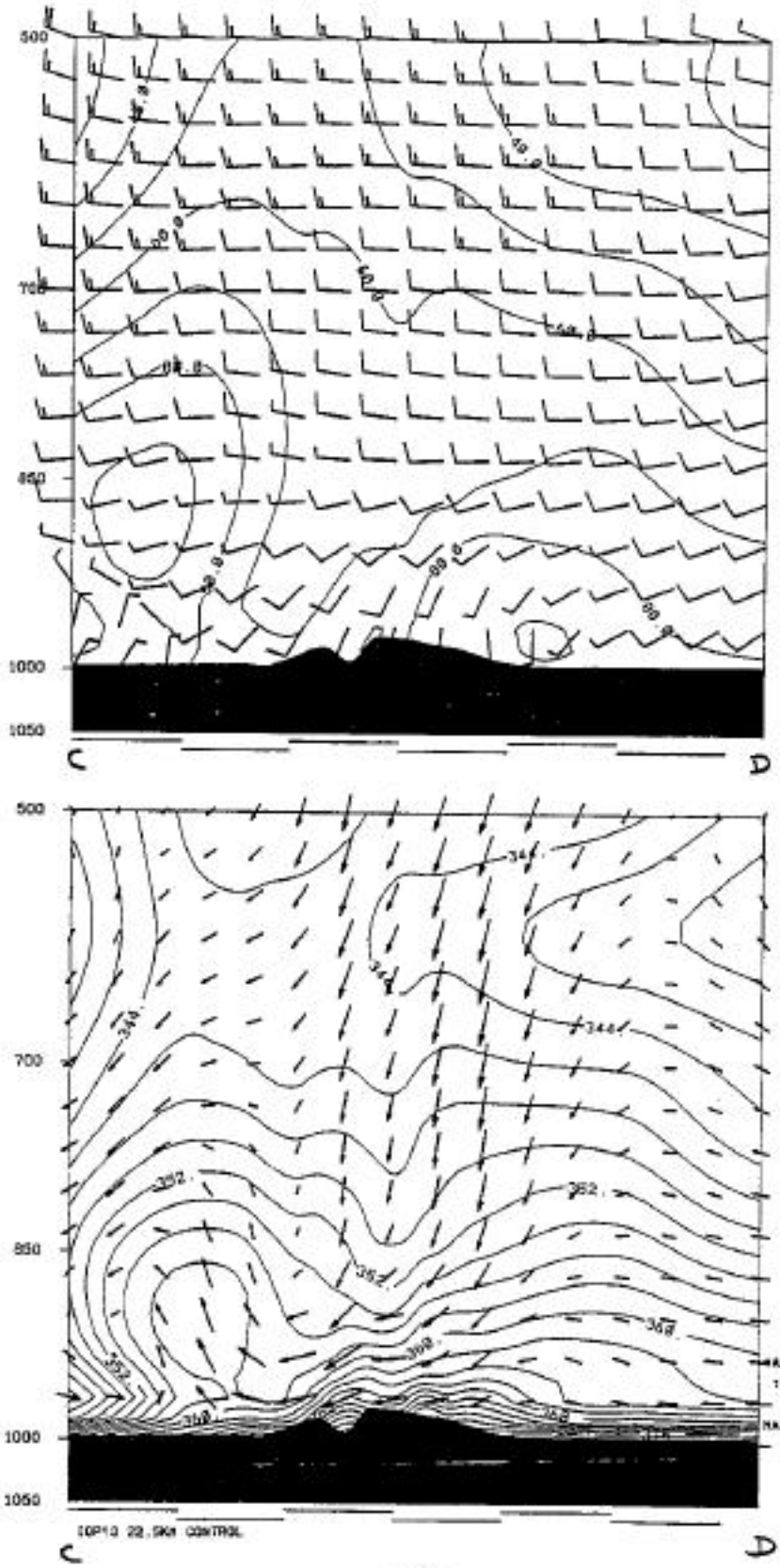
500
700
850
1000
1050
C
D
500
700
850
1000
1050
MAX HORIZ
MAX VERT
(a)
C
D

Fig. 20

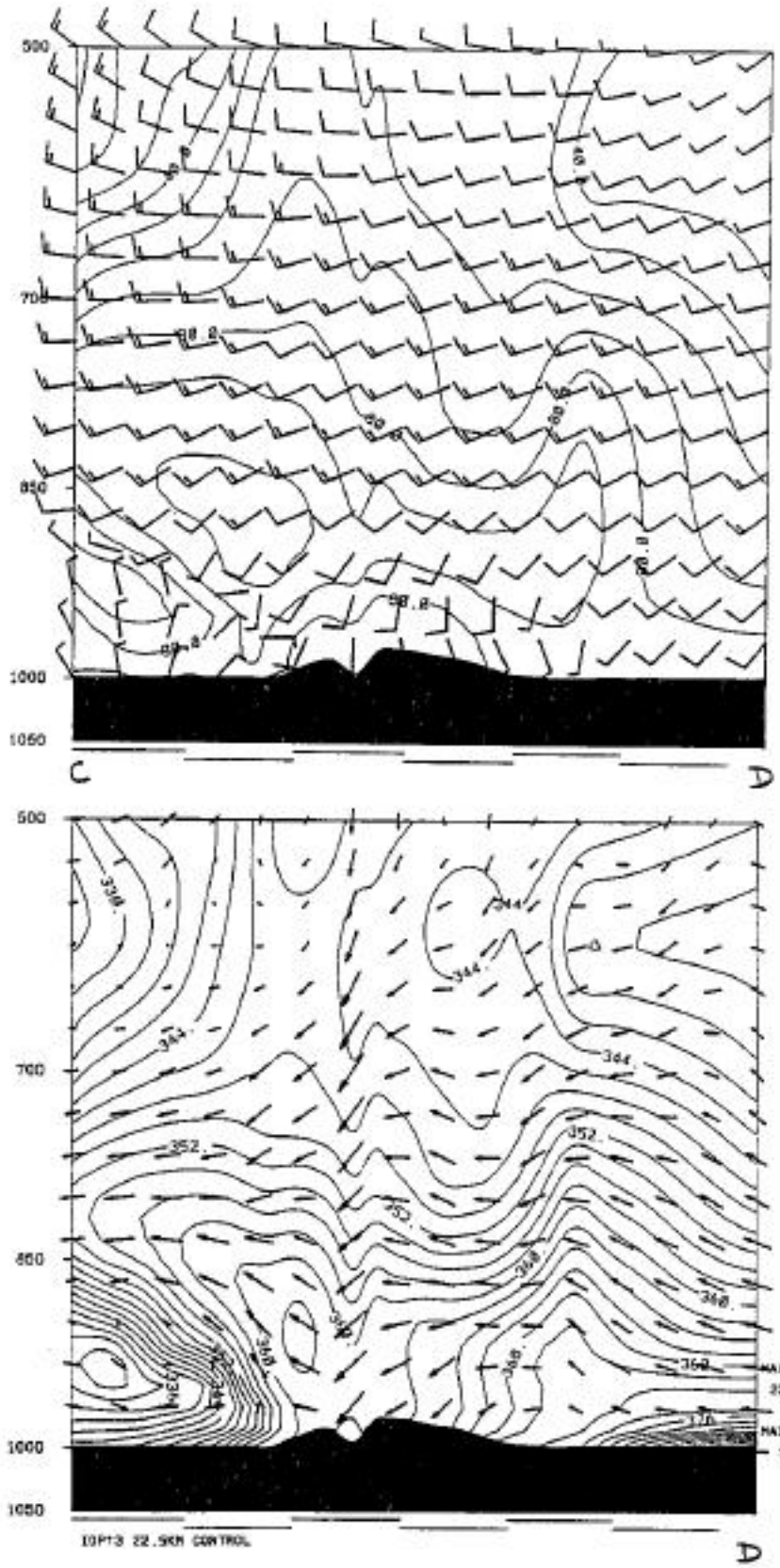

(b)

Fig. 20
Continued

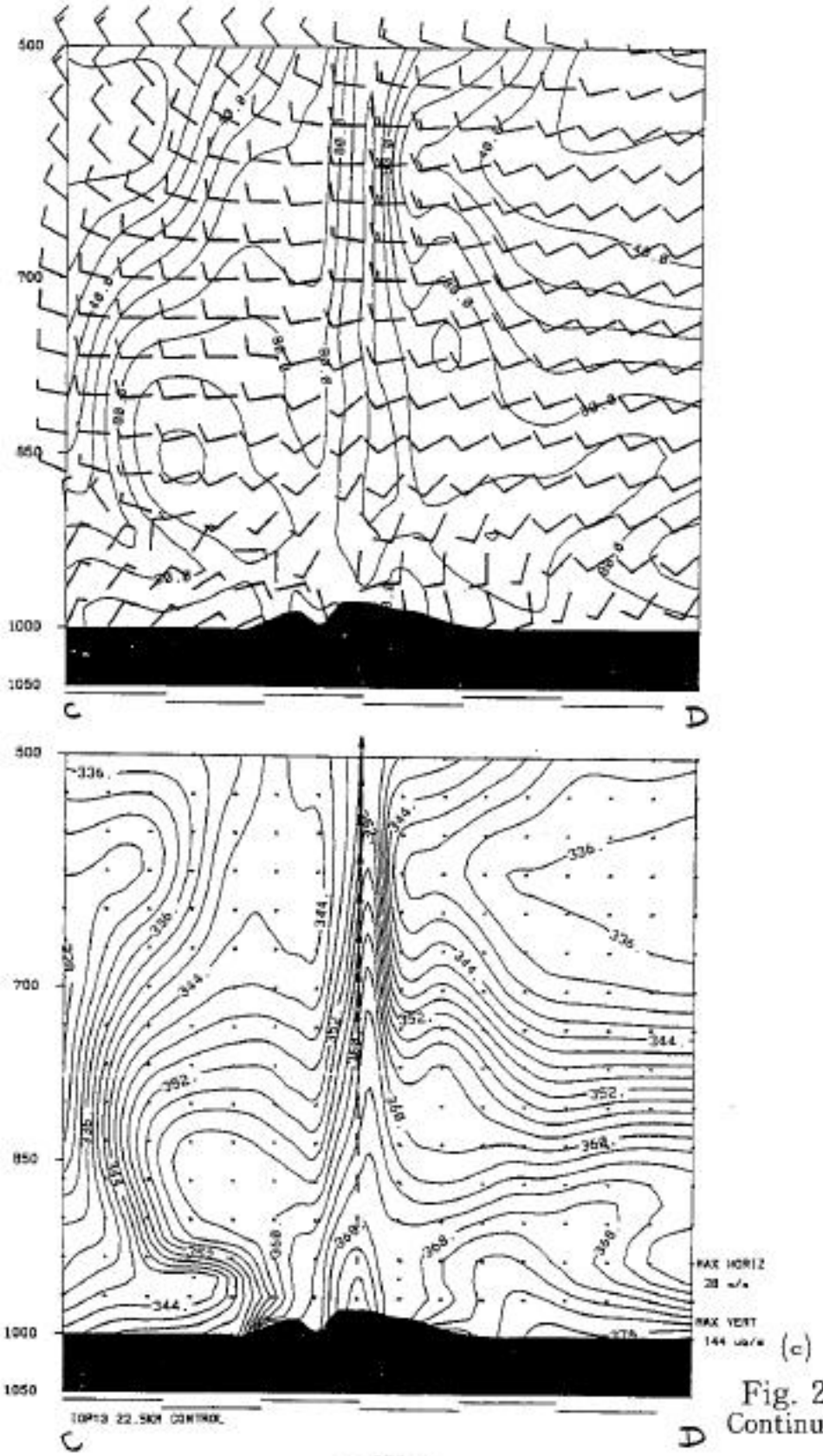

Fig. 20
Continued

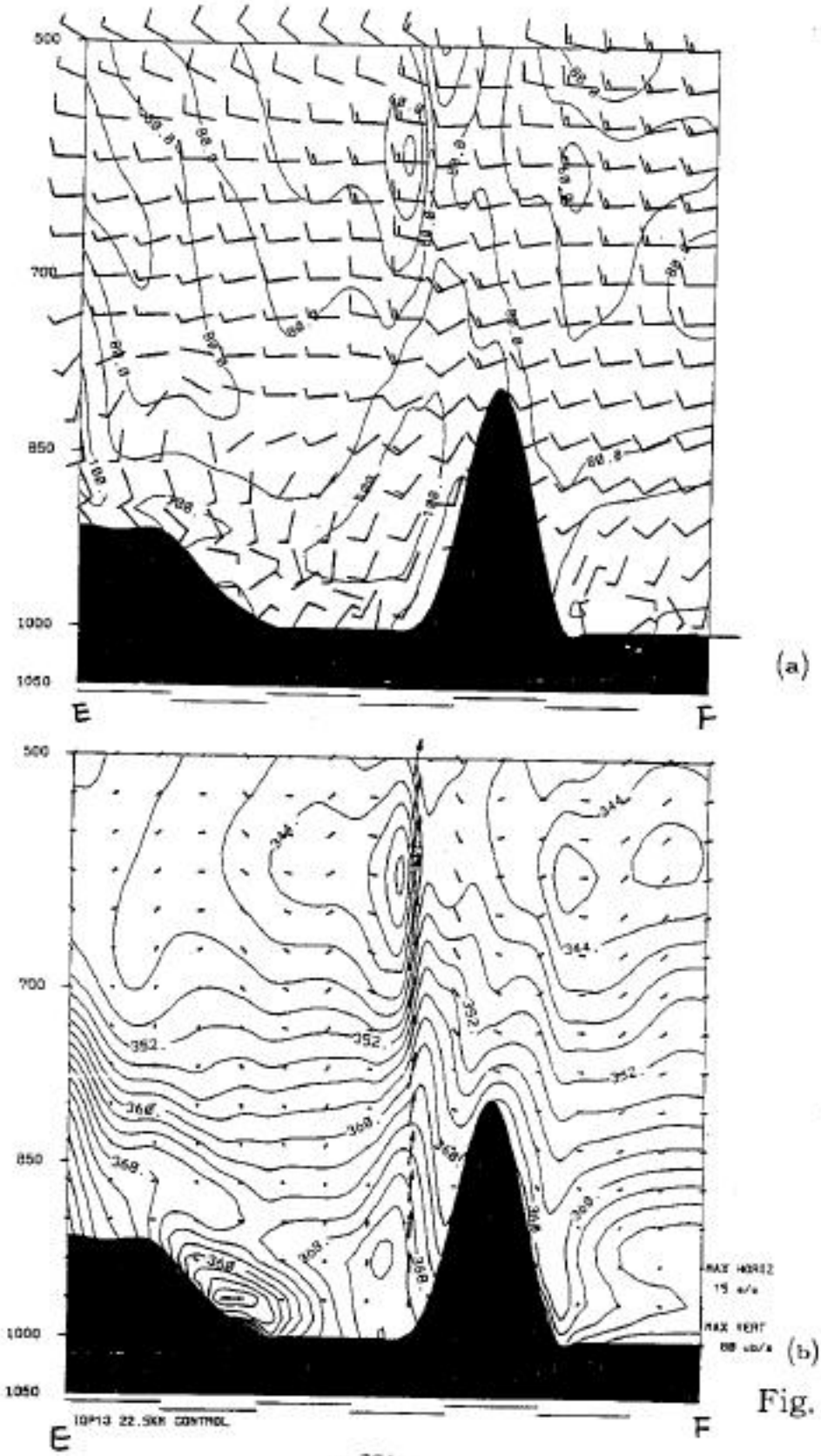

Fig. 21